Vol. 38 — N° 4 12 14 P. 441 – 466

GEOSTANDARDS and GEOANALYTICAL RESEARCH

CAMAM: A Miniature Laser Ablation Ionisation Mass Spectrometer and Microscope-Camera System for *In Situ* Investigation of the Composition and Morphology of Extraterrestrial Materials

Marek **Tulej** (1)*, Andreas **Riedo** (1), Maike B. **Neuland** (1), Stefan **Meyer** (1), Peter **Wurz** (1), Nicolas **Thomas** (1), Valentine **Grimaudo** (2), Pavel **Moreno-García** (2), Peter **Broekmann** (2), Anna **Neubeck** (3) and Magnus **Ivarsson** (4)

(1) Physics Institute, Space Research and Planetary Sciences, University of Bern, Bern, Switzerland
(2) Department of Chemistry and Biochemistry, University of Bern, Bern, Switzerland
(3) Department of Geological Sciences, Stockholm University, Stockholm, Sweden
(4) Department of Palaeobiology and Nordic Centre for Earth Evolution (NordCEE), Swedish Museum of Natural History, Stockholm, Sweden
* Corresponding author. e-mail: marek.tulej@space.unibe.ch

Performance studies of a microscope-camera system (MCS) and a laser ablation/ionisation mass spectrometer (LIMS) instrument (referred to here as a laser mass spectrometer or LMS) are presented. These two instruments were designed independently for *in situ* analysis of solids on planetary surfaces and will be combined to a single miniature instrument suite for *in situ* chemical and morphological analysis of surface materials on planetary bodies. LMS can perform sensitive chemical (elemental, isotope and molecular) analyses with spatial resolution close to micrometre-sized grains. It allows for studies with mass resolution ($M/\Delta M$) up to 800 in ablation mode (elemental composition) and up to 1500 in desorption mode (molecular analysis). With an effective dynamic range of at least eight orders of magnitude, sensitive and quantitative measurements can be conducted of almost all elements and isotopes with a concentration larger than a few ppb atoms. Hence, in addition to the major element composition, which is important for the determination of mineralogical constituents of surface materials, trace elements can also be measured to provide information on mineral formation processes. Highly accurate isotope ratio measurements can be used to determine *in situ* geochronology of sample material and for investigations of various isotope fractionation processes. MCS can conduct optical imagery of mm-sized objects at several wavelengths with micrometre spatial resolution for the characterisation of morphological surface details and to provide insight into surface mineralogy. Furthermore, MCS can help in the selection of sample surface areas for further mass spectrometric analysis of the chemical composition. Surface auto-fluorescence

L'étude des performances d'un système microscope-caméra (MCS) et d'un instrument couplant l'ablation laser et un spectromètre de masse à ionisation (LIMS) (appelé ici un spectromètre de masse laser ou LMS) est présentée. Ces deux instruments ont été conçus indépendamment pour l'analyse in situ de solides sur les surfaces planétaires et seront combinés en une seule suite d'instruments miniaturisés pour les analyses in situ chimiques et morphologiques des matériaux de surface sur les corps planétaires. Le LMS peut effectuer des analyses chimiques (élémentaire, isotopique et moléculaire) avec une grande sensibilité et une résolution spatiale proche de la taille de grains micrométriques. Il permet des études avec une résolution de masse ($M/\Delta M$) de jusqu'à 800 en mode ablation (composition élémentaire) et jusqu'à 1500 en mode de désorption (analyse moléculaire). Avec une plage dynamique effective d'au moins huit ordres de grandeur, des mesures sensibles et quantitatives peuvent être menées pour presque tous les éléments et les isotopes pour des concentrations supérieures à quelques ppb atomes. Par conséquent, en plus de la composition en élément majeur, qui est importante pour la détermination des constituants minéralogiques des matériaux de surface, les éléments traces peuvent également être mesurés et fournir des informations sur les processus de formation de ces constituants minéralogiques. Les mesures très précises des rapports isotopiques peuvent être utilisées pour la géochronologie in situ d'échantillon de matériau et pour les études de processus variés de fractionnement isotopique. Le système MCS permet l'imagerie optique d'objets de taille millimétrique à plusieurs longueurs d'onde et avec une résolution

doi: 10.1111/j.1751-908X.2014.00302.x

measurements and images in polarised light are additional capabilities of the MCS, to identify either fluorescing minerals or organic materials, if present on the analysed surface, for further investigation by LMS. The results obtained by investigations of NIST reference materials, amino acid films and a natural graphite sample embedded in silicate rock are presented to illustrate the performance of the instruments and their potential to deliver chemical information for mineral and organic phases in their geological context.

Keywords: geochemical analysis, contextual chemical analysis, *in situ*, geochronology, laser ablation/ionisation mass spectrometer, space exploration, microscope imagery, spectrophotometric analysis, isotope ratio measurements, mineralogy.

spatiale micrométrique pour la caractérisation des détails morphologiques de surface, et pour avoir un aperçu de la minéralogie de cette surface. En outre, le système MCS peut aider dans le choix des zones de surface de l'échantillon pour une analyse plus approfondie de la composition chimique grâce à la spectrométrie de masse. Des mesures d'auto-fluorescence des surfaces et des images en lumière polarisée sont des fonctionnalités supplémentaires du système MCS, qui peuvent permettre d'identifier des minéraux ou des matières organiques fluorescentes, s'ils sont présents sur la surface analysée, pour des compléments d'analyse par LMS. Les résultats obtenus pour l'étude des matériaux de référence NIST, de films d'acides aminés et d'un échantillon de graphite naturel inclus dans une roche silicatée sont présentés afin d'illustrer la performance des instruments et leur potentiel à fournir des informations chimiques sur des minéraux et des phases organiques dans leur contexte géologique.

Mots-clés : analyse géochimique, analyse chimique contextuelle, in situ, géochronologie, LIMS, exploration spatiale, imagerie microscopique, analyse spectrophotométrique, mesures du rapport isotopique, minéralogie.

Received 17 Jan 14 – Accepted 22 Oct 14

In the last few decades, the role of chemical analysis of extraterrestrial materials has increased significantly in space research as planetary orbiting and landing missions have begun to contribute substantially to the cosmochemical database (Prettyman 2006, McSween *et al.* 2011, Kim and Hasebe 2012). Several instruments on orbiting spacecraft, and on landers and rovers have been developed for the chemical analysis of planetary surfaces. While the measurements conducted on orbiting spacecraft by remote sensing instruments provide information on the chemical composition of planetary objects on a global scale, the instruments deployed on a lander or a rover are intended to measure a local surface composition (Prettyman 2006, McSween *et al.* 2011, Kim and Hasebe 2012). Typically, only small size, lightweight and power-efficient instruments characterised by a robust design and simple operation can be adopted for space research (McSween *et al.* 2011). These constraints are the main reasons why many well-established analytical techniques used in the laboratory (e.g., LA-ICP-MS, TIMS) cannot be employed in space as their adaptation to this environment would be difficult at the present stage of technology.

Recently, two new analytical instruments, the laser-induced breakdown spectrometer (LIBS) and the laser ablation/ionisation mass spectrometer (LIMS), have been designed for space research to improve the sensitivity and spatial resolution of chemical analysis. These methods allow fast measurements and do not require any sample preparation (Cremers and Chinni 2009, Lin *et al.* 2010). A LIBS instrument is currently deployed on the Curiosity rover (Grotzinger *et al.* 2012, Maurice *et al.* 2012, Wiens *et al.* 2012) and is part of the Mars Science Laboratory (MSL), while a LIMS instrument (LASMA) was included on the Phobos Sample Return mission (Managadze *et al.* 2010, Zelenyi and Zakharov 2010), which unfortunately terminated in the Earth's atmosphere in 2011. LASMA will be deployed on the lunar lander of the Luna Resurs mission (Khartov *et al.* 2011). Both LIBS and LIMS methods use a pulsed laser beam focused to a spot size of tens to hundreds of micrometres to ablate, atomise and ionise material from a sample surface. While LIBS optical spectroscopy is applied for element detection, the LIMS method provides mass spectrometric analysis of ions that are produced during the laser ablation process. For quantitative chemical analysis, the stoichiometric production of neutrals (LIBS) and ions (LIMS) should be maintained, which often can be achieved by an appropriate operation of the laser ablation source. The LIMS method is more sensitive and delivers detection of elements with concentrations down to ppb atoms levels, whereas LIBS

instruments can determine elements with concentrations of 10–100 ppm (Salle *et al.* 2005, 2007, Pavlov *et al.* 2012, Riedo *et al.* 2013a). The LIBS instrument offers, however, flexibility of operation in various environments and measurements of distant objects. On MSL, LIBS is used to investigate surface and subsurface chemical composition of samples located up to 7 m from the instrument. LIBS delivers complementary measurements to those obtained by alpha proton mass spectrometry (APXS, Cousin *et al.* 2011, Campbell *et al.* 2012), allowing a more detailed analysis of Martian surface chemistry and mineralogy. The current LIBS system applied on MSL is combined with a micro-imager camera system (Maurice *et al.* 2012). The latter is used for surface imagery to help in selection of surface areas for further LIBS investigations. The imaging system delivers the physical properties of the material and adds further constraints to the analysis of the chemical composition of the sample. The potential of such combined analyses was emphasised during instrument performance tests on the investigation of variations in the proportion of different mineral phases and the distribution of mineral grains (Cousin *et al.* 2012). Detection sensitivity of the LIBS instrument often permits the measurements of a limited number of elements with concentrations larger than 10–110 ppm only (Salle *et al.* 2004).

The miniaturisation of LIMS, necessary for the application in space research, was achieved in the last decade (Brinckerhoff *et al.* 2000, Rohner *et al.* 2003, 2004). LIMS is a well-known analytical method for investigation of the elemental and isotopic composition of solid materials. In addition, the technique can be used for the detection of molecular compounds adsorbed on solid-state surfaces (Hillenkamp 1982, Vertes *et al.* 1993). Current LIMS systems can deliver highly sensitive, accurate and precise elemental and isotope measurements (Riedo *et al.* 2013a, b, Zhang *et al.* 2013). Recent investigations also show that LIMS can be used to investigate the elemental composition of any solid without the necessity for reference materials (RM) for calibration of the measurement results (Vertes *et al.* 1993, Riedo *et al.* 2013b, Zhang *et al.* 2013).

Close-up cameras delivering images of mm-sized planetary regolith/soils are well developed in space research. In addition to visualisation of the morphological properties of planetary materials, these space instrument suites can deliver important information on the geological origin of the material and an insight into morphological characteristics (size, shape and texture) of the rocks. These instruments are also used to study physical properties of the material including optical reflectance and infrared (IR) emission. Further improvements were made by combining a microscope with the camera for investigation of the surface structure with a spatial resolution in the micrometre range (Herkenhoff *et al.* 2003, Thomas *et al.* 2004). These measurements are essential for morphological and mineralogical analyses, and in the search for biological activity on planetary surfaces (Thomas *et al.* 2004). A microscopic imager was deployed on the Mars Exploration Rovers (MER) and provided observations with a spatial resolution of around 30 μm. Data obtained from the *Spirit* and *Opportunity* rovers were used for detailed analysis of the internal structure of rock material (Herkenhoff *et al.* 2008). The Beagle 2 microscope system (MIC) developed for the Beagle 2 lander of the Mars Express mission (Chicarro *et al.* 2003) was intended to go a step further (Thomas *et al.* 2004). The objective was to search for signs of Martian life, past or present, and would have provided optical images of the Martian surface with about 6 μm spatial resolution giving the potential for an extended geophysical analysis and mineralogical interpretation of the landing site (Thomas *et al.* 2004). Unfortunately, communication with Beagle 2 was lost during the landing phase in December 2003. In addition to high-resolution optical imagery, the microscope-camera system (MCS) designed for this mission provided multi-colour images of the surface in the visible (VIS) and near-infrared (NIR) spectral ranges. The instrument could be used to conduct simple fluorescence experiments and to take images of the sample surface in polarised light. It has been shown subsequently that the instrument can deliver contextual information by conducting morphological and mineralogical analyses of rock specimens. Detection of organic compounds can be performed also by the application of UV light-induced surface fluorescence analysis (Thomas *et al.* 2004).

Here, we introduce two laboratory prototype instruments designed for space research, a miniature laser ablation/ionisation mass analyser (LMS) and a MCS. Their capabilities are summarised and discussed based on current and past measurements and in the following, the results of mineralogical measurements on a sample of graphite embedded in a silicate host rock (Ronda sample). Finally, the design of a miniature instrument suite, and chemical and morphological analyses of asteroidal materials (CAMAM), combining MCS and LMS, are presented. The CAMAM design was prepared for the MarcoPolo-R spacecraft, the ESA mission to an asteroid (http://sci.esa.int/marcopolo-r, M. Tulej, A. Riedo, M. Neuland, S. Meyer, P. Wurz and N. Thomas, in prep.).

Methods and instruments

Currently, the MCS and LMS instruments are operated independently from each other and will be discussed in

separate sections. This section provides details on the design and operation, and sample preparation method, as well as instrument figures of merit for each instrument.

LMS

The miniature laser ablation ionisation mass spectrometer, LMS, was initially developed for a lander on the BepiColombo mission to Mercury (Rohner *et al.* 2003). The design and construction of this instrument for a lander were described in a previous publication (e.g., Rohner *et al.* 2003). The status of instrument development and current laboratory configuration can be found in recent publications (Riedo *et al.* 2013a, b). Only a brief description of the set-up and instrument operation will be given here.

The LMS instrument consists of a laser ablation ion source and a mass analyser. Figure 1 (left panel) shows an image of the construction details of the mass analyser, a reflectron-type time-of-flight (ToF) mass spectrometer. The mass analyser body possesses a cylindrical symmetry (Ø60 mm × 160 mm) and a mass of about 400 g.

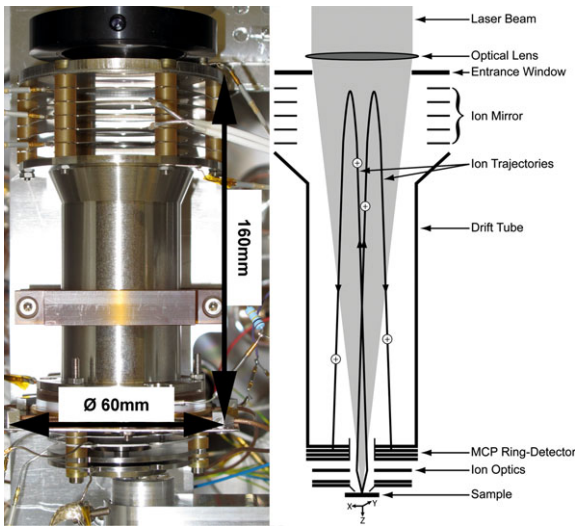

Figure 1. Left: Photograph of the laser mass spectrometer (LMS) mass analyser. The sample is mounted on the sample holder that is located near to the entrance to the mass analyser at the bottom of the instrument. Right: Schematic diagram showing the principle of operation of the LMS. Ions produced during laser ablation enter the interior of the mass analyser. Their flight trajectories are controlled by an ion-optical system. After confinement, acceleration and focussing, the ions enter the ion mirror and are reflected towards an ion detector (multi-channel plate, MCP).

An NIR fs-laser ablation ion source is implemented in the current configuration. Laser radiation is produced by an fs-laser system (λ = 775 nm; pulse width of 190 fs, repetition rate of 1 kHz). The optical system consists of a beam expander, several folding mirrors and a doublet lens, which are designed to focus the laser radiation onto the sample surface to a spot of about 10–20 μm in diameter (FWHM). Typically, for each of the investigated samples, laser power density (irradiance) is tuned to produce stoichiometric fractions of ions (Riedo *et al.* 2013b, Zhang *et al.* 2013). The optimal laser irradiances were determined from initial experiments on RM. For the laser desorption studies, we used the same experimental set-up, but the laser irradiance applied was typically 100–1000 times lower, as is common in laser desorption (Lykke *et al.* 1992, Wurz *et al.* 1992). Furthermore, desorption studies were conducted using a defocused laser beam.

Figure 1 (right panel) displays the principles of operation of the LMS instrument. The laser ablation ion source generates an ion cloud above the sample surface, just at the entrance to the mass analyser, for each laser pulse. Only positively charged ions subsequently enter the interior of the mass analyser where they are confined, accelerated and focused by the ion-optical system. Mass separation occurs during the flight to an ion multi-channel plate detector (MCP) and is performed in two field-free sectors (drift tube) of the reflectron-type ToF mass analyser. An axially symmetric grid-less reflectron is used to improve the performance of the ToF analyser (e.g., ion transmission) and supports a light and compact design of the instrument. A custom-designed ion detector with two microchannel plates mounted in a chevron configuration and with a multi-anode read-out is used to measure ion bunches as a function of their arrival time, with an effective dynamic range of at least eight orders of magnitude. The charge pulses collected on the anode segments are sent to the analogue-to-digital converter (ADC) system and are collected by the data acquisition system to form a ToF mass spectrum. Typically, a mass spectrum in the range 1–250 dalton was recorded within ~ 15 μs after the laser pulse that initiated the ablation process. The transformation from the time of flight spectrum into mass spectrum is simple, and an accuracy of the mass scale of 500 ppm was achieved (Riedo *et al.* 2013a). Implementation of a computer-controlled optimiser allows reproducibility and stability of the instrument (Riedo *et al.* 2013a). At optimal conditions, the LMS mass resolution $M/\Delta M$ exceeds 800 (measured at ^{56}Fe, Tulej *et al.* 2011, Riedo *et al.* 2013a), which is sufficient for separating elements/isotopes, but not high enough to resolve possible isobaric interferences.

With high repetition rates (1 kHz), mass spectrometric measurement is accomplished in less than a minute. The scientific data acquisition system digitises signals at 10-bit vertical resolution at sampling rates of up to 1 GS s^{-1} in dual channel mode or 2 GS s^{-1} in single channel mode (Phobos Grunt, Luna Glob heritage). The acquisition system supports a sequential data accumulation of up to several tens of thousands of single laser-shot mass spectra and allows saving these data in files continuously over the defined time of the experiment. The accumulation time can be defined in time sequences (time evolution) for a systematic investigation of surface and subsurface. A time of individual accumulations defines, for instance, the thickness of ablated layers and the vertical resolution of the analysis. Laboratory practice shows that measurements averaged over thousands of individual laser shots are needed for good quantitative analysis performed at the same sample location. The analysis is conducted by accumulation of 20–30 data packets obtained by adding 2000 single laser-shot mass spectra. For geological samples, this yields typically to the ablation of a surface layer of a few tens to a few hundreds nm thickness for each packet (Riedo *et al.* 2013a, b). By repeating the analysis at the same sample spot, the elemental composition of a sample can be studied layer by layer to greater depths. The accumulation times can be set by command to accommodate different measurement scenarios and to optimise a balance between vertical resolution and data accumulation rate. Tables 1 and 2 give an overall summary of the characteristics of LMS and the currently used fs-laser ablation ion source.

The ion-optical and mechanical design of the LMS in the CAMAM suite (Figure 1) benefits substantially from the first design performed for the BepiColombo mission to Mercury (Rohner *et al.* 2003, Riedo 2014), the Rosetta mission (Balsiger *et al.* 2007), and from current missions to the Moon, LUNA Glob and LUNA Resource (Wurz *et al.* 2012a, b). The current LMS system represents the lightest and most powerful laser ablation mass analyser built for space research.

MCS

MCS is an optical microscope combined with a monochrome CCD camera. The MCS prototype is displayed in Figure 2. MCS records multi-colour imagery with a resolution of 1 μm per pixel while viewing a 2 mm × 2 mm surface. The optical system is equipped with a subsystem delivering images of the surface in polarised light. Optionally, MCS can be used for investigation of the sample fluorescence induced by UV illumination

Table 1.
Overview of the laser mass spectrometer

Quantity	Value
Mass	1.5 kg (mainly electronics)
Dimensions	160 mm × Ø60 mm
Power consumption	7 W (ion optical and acquisition system)
Laser wavelength	IR
Laser pulse length	190 fs
Spatial resolution	
Lateral	~ Ø 10–20 μm
Vertical	Optional: 10 nm per laser pulse
Depth	Optional: ~ 50 μm
Dynamic range	> 10^8
Mass range	1000 dalton
Mass resolution, $M/\Delta M$	Typically 800, measured at ^{56}Fe
Detection sensitivity (elements)	Tens of ppb
Detection sensitivity (molecules)	in ppm range
Isotope measurement accuracy	‰-range
Number of possible active channels	4
Time-of-flights	20 μs, lead at ~ 15 μs
Voltage applied on detector	~ 2 kV
Voltages applied for ion optical system	< 2 kV
Analogue-to-digital converter (ADC) sampling rates	1 GS s^{-1} dual and 2 GS s^{-1} single channel mode
ADC vertical resolution	10 bit

Table 2.
Overview of the characteristics of laser ablation/desorption ion source

Laser characteristics	Range of applicable values
Power density (ablation mode)	~ 0.5–5 TW cm^{-2}
Power density (desorption mode)	0.5–5 GW cm^{-2}
Laser focus diameter	5–40 μm
Spatial profile	Gaussian (top hat)
Pulse duration	~ 190 fs
Repetition rate	≤ 1 kHz

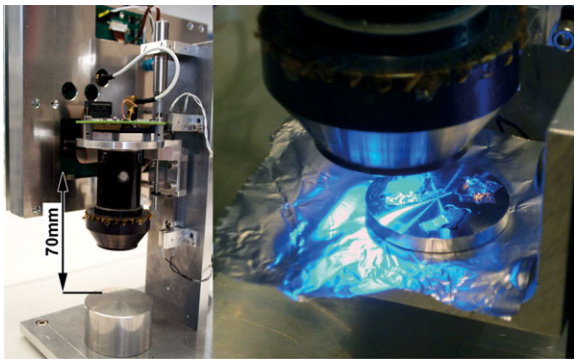

Figure 2. Left: Image of the MCS prototype. Right: Image of the head of MCS and sample holder taken during the measurements of a sample material using blue light illumination.

of the surface. The depth of focus of the optical microscope is close to about 40 μm, and with reduced image quality, the analysis of the surface can also be conducted within ± 250 μm (Lüthi 2008).

The samples are illuminated by light-emitting diodes (LED) of different colours (red, green, blue), which are embedded in the MCS head. LEDs can be switched on and off individually. The baseline detector chosen for MCS is an Osprey-2k, Raytheon Si-PIN Array, which consists of 2048 × 2048 pixels and offers high-performance operation. The custom-designed read-out electronics are accommodated in a 3D package. A similar design was implemented successfully in the Rosetta-CIVA and in the Beagle-2 lander microscope (MIC), which flew on the Mars Express mission (Thomas *et al.* 2004). The optical head assembly is similar to the original MicrOmega/VIS channel; however, this channel for ESA's 2018 ExoMars was descoped because of mass limitations at system level. The interface tube provides a link from the optical to the microcamera head. Two microfilters for venting the interior of the microscope and preventing penetration of particles larger than 1 μm were incorporated. The microscope can be operated in a nominal temperature range -40 °C to +30 °C. A single thermistor is included to control working temperatures during nonstop measurements. Table 3 gives an overview of the MCS characteristics.

Table 3.
Summary of MCS characteristics

Quantity	Value
Mass	190 g
Volume	115 mm × 65 mm × 55 mm
Image scale	1 μm per pixel
Field of view	2 mm × 2 mm
Working distance	12 mm
Detector type	Osprey-2k/Raytheon
Peak	Quantum efficiency > 80%
Detector size	2048 pixel × 2048 pixel
Pixel Pitch	10 μm (square)
Digital resolution	14 bit
Optics	Cook Triplet
Depth of field	40 μm (± 250 μm with reduced quality)
Focusing mechanism	Fixed distance
Front window	Sapphire
Illumination	12 bulbs or LEDs
Spectral resolution	4 colours (blue, orange, red, near-infrared), (480, 560, 700, 830 nm), Bandwidth 30–100 nm
Other features	UV illumination, light polarisation capabilities
Typical exposure times	1 s
Operational temperature range	-40 °C to +30 °C
Non-operational survival temperature range	-80 °C to +60 °C

The microscope-camera system is the laboratory prototype of the instrument, which was designed for the Pasteur Instrument Payload of the ExoMars Mission and represents an example of the further developed space MCS built for the Beagle 2 mission. The latter instrument combined microscopy and VIS/NIR reflectrometry and also supports IR spectral analyses of sample surfaces.

MCS is based on LED technology and is similar to the microscope-camera system *Mahli*, currently used on the Curiosity rover. In comparison with the MCS system, Mahli has a lower resolution of 14.5 μm per pixel; however, the depth of focus is considerably larger for Mahli, which provides some operational advantages.

Samples and reference materials

The LMS instrument performance was investigated by conducting measurements on three different NIST certified reference materials (NIST SRM 661, 664 and 665). Samples of these were cut using a diamond cutter and glued on the sample holder using silver epoxy. A cylindrical piece of stainless steel was typically used as a sample holder for both LMS and MCS measurements.

The capabilities of the instrument for the detection of organic compounds were tested on samples of glycine amino acid and toluene. The glycine samples were prepared using the following procedure. Glycine (Gly) was incubated in a 6 mol l^{-1} HCl solution at 115 °C for 2.5 hr in a sealed ampulla. The treatment of glycine in highly concentrated HCl was chosen to prevent any polymerisation of the amino acid (Majer *et al.* 1981). A 1 ppm stock solution of this amino acid solution was prepared, from which 50 μl were dropcast on a defined area of the silica-supported gold wafer. The toluene reference sample was prepared the same way, by dropcasting 50 μl of a 1 ppm stock solution on a different gold substrate. Both samples were exposed to an Ar-atmosphere to evaporate the solvent, which resulted in a total mass of 0.05 μg glycine and toluene, respectively, absorbed on ~ 0.5 cm^2 gold support. The implemented sample preparation is a promising procedure in terms of simplicity and reliability, and possibly can be used for *in situ* space research applications. Glycine (ReagentPlus, ≥ 99%, TLC) was purchased from Sigma-Aldrich (Steinheim, Germany), H_2SO_4 (VLSI Selectipur 96%) from BASF (Ludwigshafen, Germany) and HCl (GR for analysis, 25%) as well as toluene (GR for analysis) from Merck (Darmstadt, Germany). Samples of glycine and toluene films attached to the holder are displayed in Figure 3 (right panel).

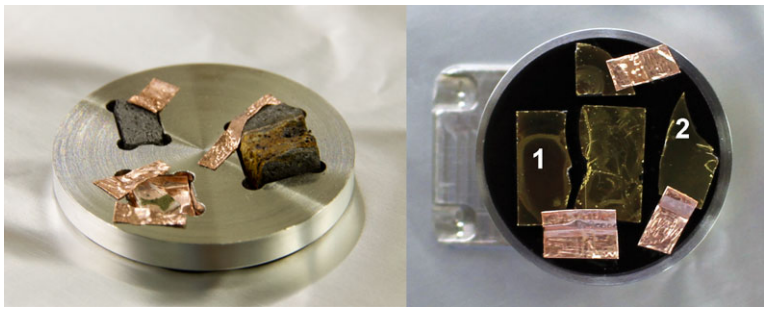

Figure 3. Left: Various samples attached to a sample holder with Cu tape for ultra-high-vacuum (UHV) applications. The largest sample, which is seen on the right side of the sample holder, is a sample of graphite embedded in serpentinised peridotite. This sample is investigated in the last section of the paper by both MCS and LMS. Right: Samples of amino acid films deposited on gold-coated silicate substrates are attached to the sample holder with copper tape for UHV applications. The samples No. 1 (glycine) and 2 (toluene) were used in the current laser desorption investigation.

Two natural rock samples collected from the 'Los Pobres' graphite mine (Spain) (see Figure 3, left panel) were investigated (see below). The sample was cut into approximately 1 cm^2 pieces with a diamond saw and mounted onto the sample holder with copper tape. The graphite was found within a serpentinised outcrop of peridotite (host rock) in Serranía de Ronda (southern Spain).

Measurement procedure

LMS: Untreated samples were used for the investigations, and no sample cleaning was undertaken. The samples located on the sample holder were placed in a small vacuum chamber, which was attached to the main experimental vacuum chamber. After evacuation, the sample was transported from the small chamber to the experimental chamber by a sample introduction system (Riedo 2014). The laser ablation technique and the experimental procedure of measurements allow the determination of the chemical composition of any solid sample. Possible contamination of the sample by dust particles and the presence of surface layering (oxidation layer) due to contact with the atmosphere or other interfaces did not cause problems, because the uppermost surface layers of the sample were removed (or analysed) systematically. This was achieved through depth profiling of the sample surface. With the current set-up, a sample surface of ~ 15 µm in diameter can be analysed layer by layer with a depth resolution down to a few nanometres (Table 1). Although the range of laser irradiances suitable for quantitative analysis is often well defined by investigations of various RM samples, the specificity of each sample (optical properties) requires fine adjustment of the laser ablation ion source to achieve optimum instrument performance. The rate of material removal by the focused laser radiation depends on the surface composition and the applied irradiance (fluence). Initial fluence test measurements were prepared by applying a range of laser fluences to select optimal measurement conditions when very different samples were investigated (e.g., metals, rocks, glass or powders). The applied laser fluences/irradiance for investigation of such materials were collected in the data base and used in future studies without repeating laser fluence campaigns. Typically, the fs-laser ablation source offers robust operation and quantitative measurements in the large range of laser fluences/irradiances applied (Zhang *et al.* 2013). A fs-laser ablation ion source allows clean sample ablation without formation of ablation pits and rims. Due to its short pulse duration, no interaction with plasma formed during the ablation can occur. This is essential to reduce element fractionation effects substantially (Russo *et al.* 2013). Hence, the operation of the laser ablation ion source is suitable for stoichiometric ion production.

Figure 4 shows the graphite host rock mass spectra recorded with iteratively increasing laser fluence. Each measurement was conducted at one sample location, and thirty data files were recorded, each obtained by summing continuously 2000 single laser-shot spectra. The mass spectrometric analyses of intermediate data files showed no significant variation of the intensities between the individual mass peaks except that of the first five data files. We established this procedure in previous studies taking into account the effects of a fresh surface and its contaminations (Tulej *et al.* 2012, Riedo *et al.* 2013a). Nevertheless, the systematic decay of the intensity of all mass peaks was observed during the measurement. Hence, the spectra shown in Figures 4 and 5 were obtained by summing up

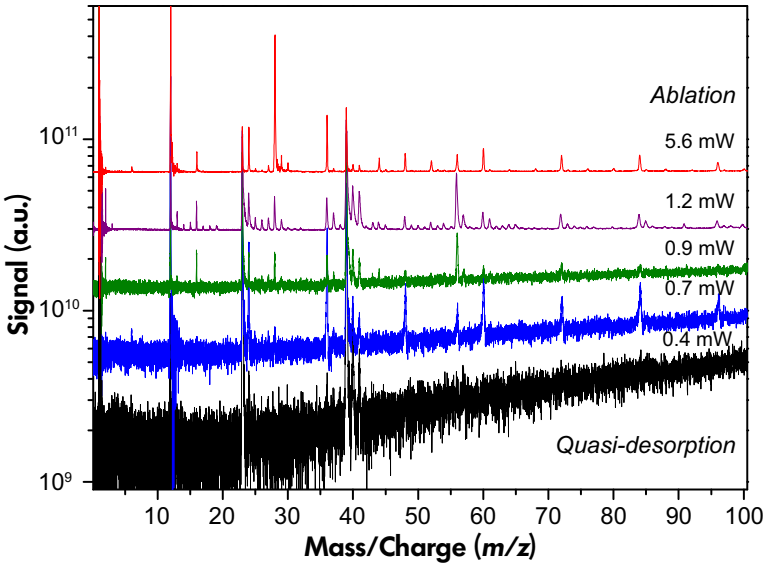

Figure 4. Mass spectra of the silicate host rock of the graphite sample (Ronda) recorded at several laser fluences. The laser fluence used for recording the uppermost spectrum was selected to conduct the quantitative elemental/isotope determination of the sample delivered in the Results and discussion section (Riedo *et al.* 2013b).

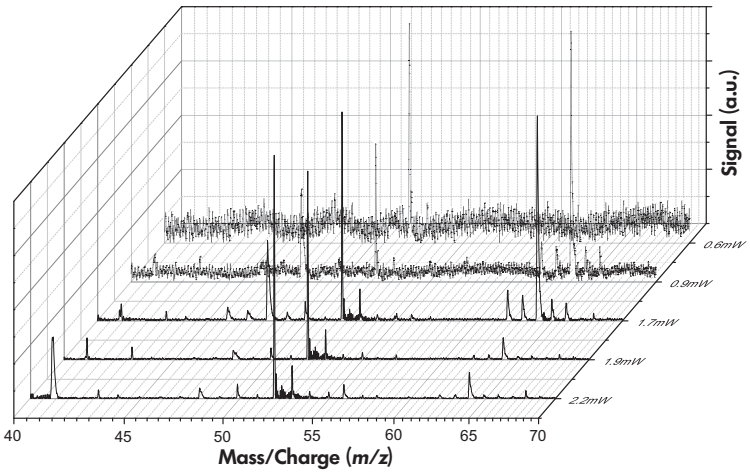

Figure 5. Laser desorption mass spectra of a toluene sample deposited on a gold-coated silica wafer recorded for various laser fluences. Laser fluences were about 100–1000 times smaller than for typical investigations by applying the laser ablation method. Typical mass resolution ($M/\Delta M$) exceeded 1000 at mass 54. The measured mass spectra indicate that molecular fragmentation could not be avoided by the fs-laser desorption method.

50000 individual single shot mass spectra, as described above.

Figure 4 shows an example of the results obtained in such a preparation study. Several mass spectra of the graphite sample, recorded from its silicate host phase, are displayed. For relatively low laser irradiance (black trace at the bottom of the Figure 4), only mass peaks of C (m = 12) (main element in the sample), Na (m = 23) and K (m = 39 and 41) were observed. The ablation thresholds for most other elements were not reached. By increasing the irradiance mass peaks of C_n (n = 1, 2, ... 8), carbon clusters at m = 24, 36, ... 94 became apparent as well as small mass peaks of Si (m = 28) and Fe (m = 56) (trace second from bottom in Figure 4). Subsequently, for an irradiance larger than ~ 1 mW, all the main elements (but also clusters) were observed, including O (m = 16), Mg (m = 24), Ca (m = 40) and CH (m = 13), CH_2 (m = 14), OH (m = 17),

OH_2 (m = 18), OH_3 (m = 19), H_xC_y (x = 1,2, ... 4; y = 1, 2, ... 21)), O_xC_y (x = 1, 2; y = 1, 2, ... 21), SiO (m = 44) and SiOH (m = 45). The analysis of the spectra indicates that reduction of the clusters and best measurements of element and isotope compositions could be achieved by the application of a specific laser fluence (> 6 mW, crater diameter of about 15–20 μm). The upper limit of the laser fluence determined from these studies was frequently a compromise between mass spectral quality and analytical performance of the instrument (due to space charge effects mass peaks can broaden and mass spectrometric resolution was reduced). In the example shown in Figure 4, the uppermost laser fluence of 5.6 mW (crater diameter of 17 μm) was selected for further investigation of the host rock sample.

Note that even when the sample was very close to the entrance of the mass analyser, contamination effects due to possible ion sputtering on the entrance skimmer body were not observed. Secondary ions possibly produced in such a process were not detected by our system (coincidence measurement), and secondary material possibly deposited again on the sample was probably of too low concentration to make these effects measurable. Furthermore, if these effects were present, a larger shift between separate sampling locations could be applied. An alternative solution would be to keep the inlet to the mass spectrometer far from the sample (Li *et al.* 2012).

A similar method was used for the investigation of organic compounds by laser desorption. For selection of laser desorption conditions, care was taken to keep the laser fluence below laser ablation threshold (when the first mass peaks of elements are observed), and sufficiently low to avoid excessive fragmentation of molecules. Figure 5 summarises the results of the laser desorption study on a toluene sample deposited on a gold-coated silica wafer. Toluene was chosen as a reference molecule for this case study due to its chemical simplicity and affinity with metal substrates, which allows it to be measured in UHV at room temperature (Friend and Muetterties 1981, Tsai and Muetterties 1982, Rauscher *et al.* 1991, Nakazawa and Somorjai 1993, Wetterer *et al.* 1998, Libuda and Scoles 2000).

MCS: Untreated samples were used for the investigations, and no sample cleaning was undertaken. The samples were kept on the same sample holder as used for LMS measurements and placed in front of the microscope entrance. For simplicity, a z-micro translational stage was used for the accurate positioning of the sample surface in front of the microscopic system.

Once the sample was positioned, RGB images were manually captured in sequence by selecting the desired LED illumination and by setting the user selected acquisition time (depending on surface characteristics, e.g., reflectivity). In-house software was used for communication with the microscopic system, for example to set the acquisition time. Each captured image was stored on the host computer. Once the RGB images are taken, commercially available software (e.g., Photoshop etc.) can be used to make a true composite image.

Results and discussion of performance studies

Performance studies of LMS

NIST SRM 661, 664 and 665: NIST SRM 661, 664 and 665 are metallic CRMs consisting mainly of Fe at various concentrations and a number of other metals and non-metals. They were used to test instrument performance for quantitative elemental and isotope determination. The studies on NIST SRM 661, 664 and 665 samples were conducted in a similar fashion, previously reported by Riedo *et al.* (2013a, b). A fs-laser ablation source (775 nm, ~ 190 fs) used in the current study was equipped with a doublet lens to focus the laser radiation to a spot size of about 10 μm in diameter. An effective dynamic range larger than 8 decades was determined from the mass spectrometric analysis of the low-gain (LG) and high-gain (HG) channels. In the latter channel, the mass spectra were recorded with a sensitivity > 100 times that of the LG channel, but at the expense of saturation of the most intense peaks in the mass spectrum. The HG channel was used for detection and quantitative measurements of elements with concentrations down to a few ppb (Riedo *et al.* 2013a, b).

The mass spectrometric analysis was conducted on statistically well-averaged data. The typical element fractionation effects observed when a ns-laser ablation ion source was applied (e.g., metallic versus nonmetallic element detection efficiencies) were substantially reduced by applying a fs-laser ablation ion source. Figure 6 shows a correlation graph between the concentration values determined from the mass spectrometric analysis of NIST samples and certified element concentrations. Relative sensitivity coefficients (RSCs) determined in these measurements were found in the range 0.2–2, similar to the values reported recently by other researchers (Zhang *et al.* 2013). For more accurate quantitative measurements, additional calibrations using material with a chemical composition similar to that of the investigated sample can be conducted to derive improved RSCs, thus accounting for matrix-dependent

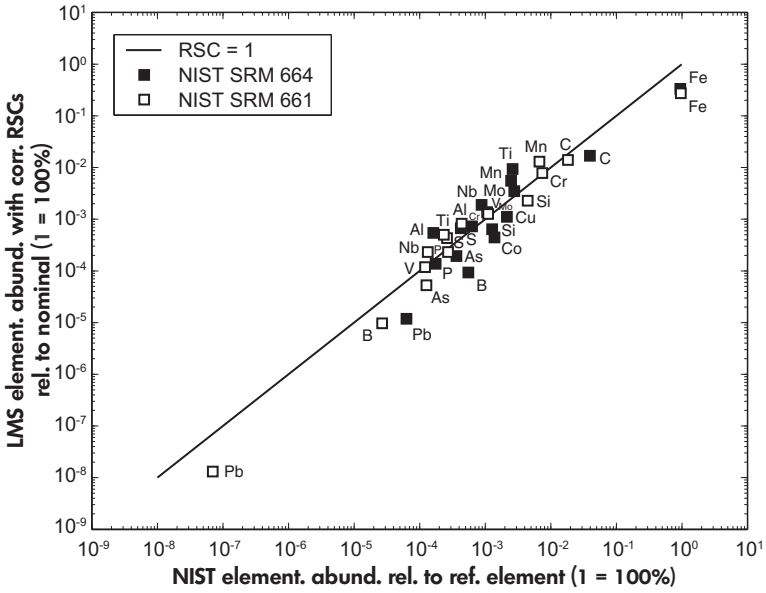

Figure 6. Correlation between the certified concentrations of elements from NIST and concentrations determined from the LMS mass spectra. For the quantification, peak areas were used. The precision and accuracy of the values were determined at 10–30% of the actual value.

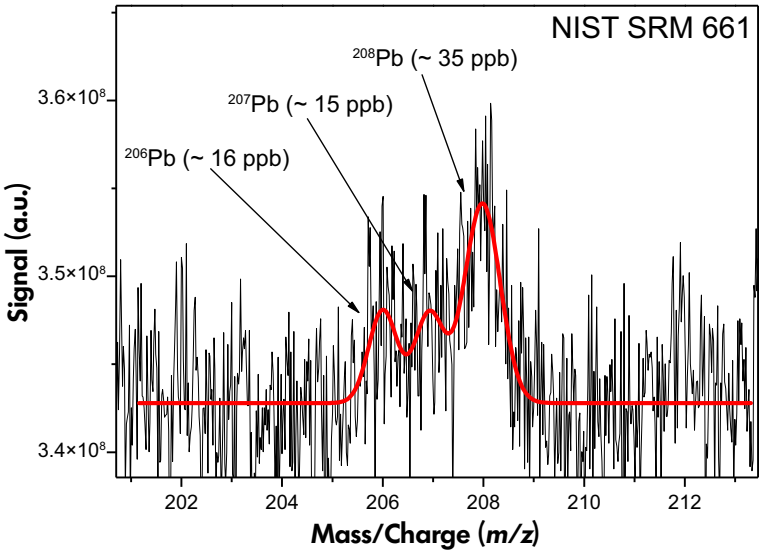

Figure 7. Section of a mass spectrum recorded for NIST SRM 661, which displays Pb isotope components determined in the sample. The thin line shows the recorded raw data, whereas the thick line, the fit of the Pb mass lines.

fractionation (Zhang *et al.* 2013). With the support of the results obtained by the mass spectrometric analysis of certified RM, the LMS could be used to conduct chemical analyses without additional RM being analysed in parallel with the sample. For the investigation of our mineralogical sample, which is presented in the next sections, the measurements of major elements were made without using scaling factors because RSCs of Mg, Al, Si, Mg, S, Ca and the majority of metallic elements were close to 1 (see also Riedo *et al.* 2013b, Zhang *et al.* 2013).

Figure 7 shows a section of the mass spectrum of a NIST SRM 661 test portion with detection of the Pb isotopes at the level of tens of ppb.

In previous studies, a direct correlation between isotope abundance and relative measurement accuracies was observed. The best accuracies for isotope measurements were observed at the per mil level and better for isotope concentrations > 100 ppm. For isotope concentrations less than ~ 1ppm, the accuracies of the measurements are in the range of tens of per cent (Riedo *et al.* 2013b). Isotope determinations performed in these studies for several elements using the mass spectra recorded for NIST SRM 661 showed an improvement in the accuracies of the isotope ratio determination. Figure 8 compares the measured values of Ti, Cr and Pb isotope ratios with the results obtained in previous studies (Riedo *et al.* 2013b). The measurement accuracies of isotopes were improved by about a factor of ten, which mainly follows from an improvement in measurement sensitivity.

Typical measurements of the reproducibility of the relative isotope ratio accuracy are demonstrated for ^{46}Ti (abundance ~ 19 ppm) measured in the NIST SRM 661 sample. A laser irradiance of about 2.6 TW cm^{-2} was used, and 56000 single laser-shot mass spectra were acquired from each of the ten surface locations. The standard deviation of all ten measurements was about 5.1‰ (Figure 9), which is about two times better than the accuracy of the measured isotope abundance ratio of about 10‰ (Figure 8). The rectangular area in grey in Figure 9 corresponds to the mean ± 1*s* of these ten measurements.

The LMS system has the potential and capability to investigate isotope fractionation in natural samples. This can result in the enhancement of the low mass isotope component of biorelevant elements (e.g., ^{12}C, ^{32}S) due to biological

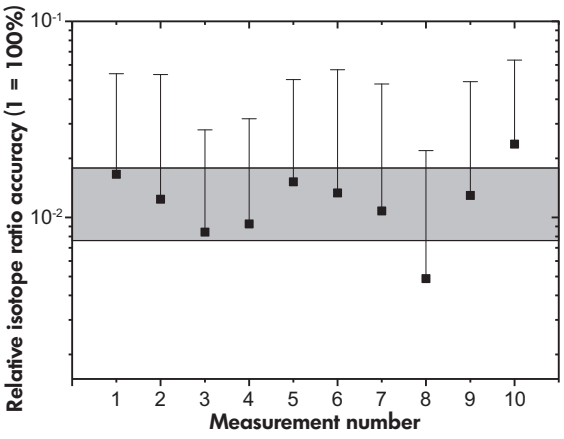

Figure 9. Relative isotope ratio accuracies of ^{46}Ti determined from ten measurements on a NIST SRM 661 sample. The grey rectangle corresponds to the mean of the measurements plus/minus one standard deviation. The standard deviation of these ten measurements was about 5.1‰, which is two times better than the accuracy of the measured isotope abundance ratio of about 10‰ (see Figure 8).

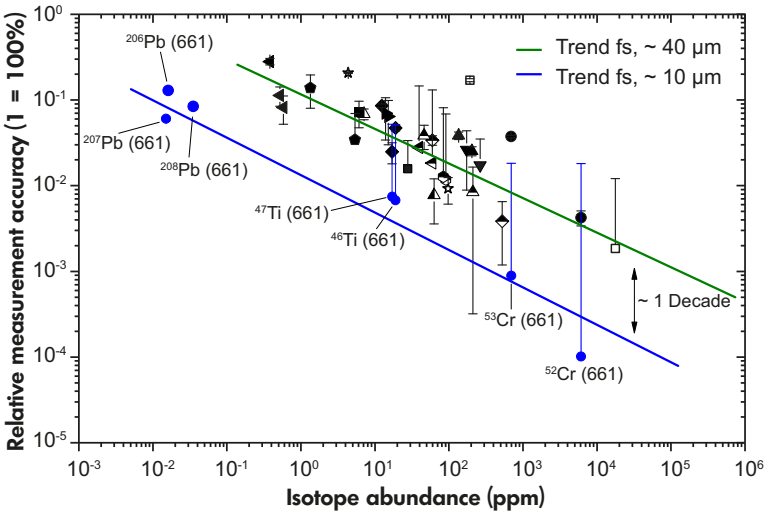

Figure 8. Correlation plot of relative measurement accuracy of isotope ratios determined from LMS spectra as a function of certified isotope concentration in the NIST SRM 661 sample. The previous measurements (Riedo *et al.* 2013c) (green, upper line) were conducted with a laser spot size of about 40 µm, and current measurements (blue, lower line) were performed with a laser spot size of about 10 µm.

activity or fractionation of isotope ratios due to radiogenic decay (e.g., Pb isotope daughter of U and Th). The accuracy of the studies can be estimated once the concentration of relevant elements and their isotopes is known. *In situ* geochronology or other measurements, where determination of isotope ratios is of importance, can be performed rapidly if a 1 kHz repetition rate of the laser ablation ion source is used. For mass spectra obtained by summing 60000 single laser-shot spectra (typically used in our analysis), an operation time of only 1 min was needed. These performance studies show that under favourable experimental conditions, the LMS instrument can achieve highly precise and accurate measurements of elemental and isotopic composition suitable for highly sensitive compositional analysis (Tulej *et al.* 2011, Riedo *et al.* 2013a–c).

Laser desorption studies of glycine and toluene deposited on solid surfaces: LMS can be used to investigate molecular compounds deposited on solid surfaces (Riedo *et al.* 2010). For such investigations, laser power densities about thousand times lower compared with ablation conditions have to be applied. Figure 10 displays a laser desorption mass spectrum for glycine and toluene deposited on a gold-coated Si wafer. The overall molecular fragmentation pattern measured for these molecules is relatively complex despite the fact that care was taken to apply the lowest possible laser irradiation during the analysis. The sample preparation procedure (STM standard cleaning procedure – well known in electrochemical studies) assured that no other molecules were deposited on the surface. The cleaning procedure employed (immersion of the sample substrate in caroic acid (75% H_2SO_4 and 25% H_2O_2), thorough rinsing with Milli-Q water, annealing for 3 min in a butane flame and cooling under an argon atmosphere prior to the dropcasting of the sample) prevents the deposition of contaminants on the surface (Kibler 2003). Nevertheless, reactions between the fragments that are produced during laser desorption can occur and cause additional complexity to the spectral assignment.

The preliminary analysis of the mass spectra measured for distinct laser fluences led to the determination of several characteristic species generated in LMS desorption mode. In principle, this approach can be applied for the detection of glycine in chemically simple environments. Figure 11 displays typical mass spectra of glycine and toluene measured in desorption mode with possible fragment products. A promising marker for a peptide bond in amino acids could be the product ion g (m/z = 55), which was not observed in the reference spectrum. However, in this study, we observed several mass peaks that could not be assigned to a single species (e.g., a*, b*, d* and h*) (see Table 4). We point out that the assignment of amino acid-derived fragments is at this stage not conclusive due to the unknown plasma chemistry; this needs to be explored further by more elaborate experiments.

The fs-laser desorption method applied here is a relatively new technique in which the mechanism of molecular desorption is not well understood and is the subject of current research (Cui *et al.* 2013). The studies presented here are preliminary fs-laser desorption investigations, and identifying the relevant desorption/fragmentation mechanism, which could explain the rather complex fragmentation patterns observed for glycine and toluene, is not straightforward. In the case of the glycine sample, its deposition on the surface followed the formation of polyglycine. Hence, the application of higher laser fluence would be

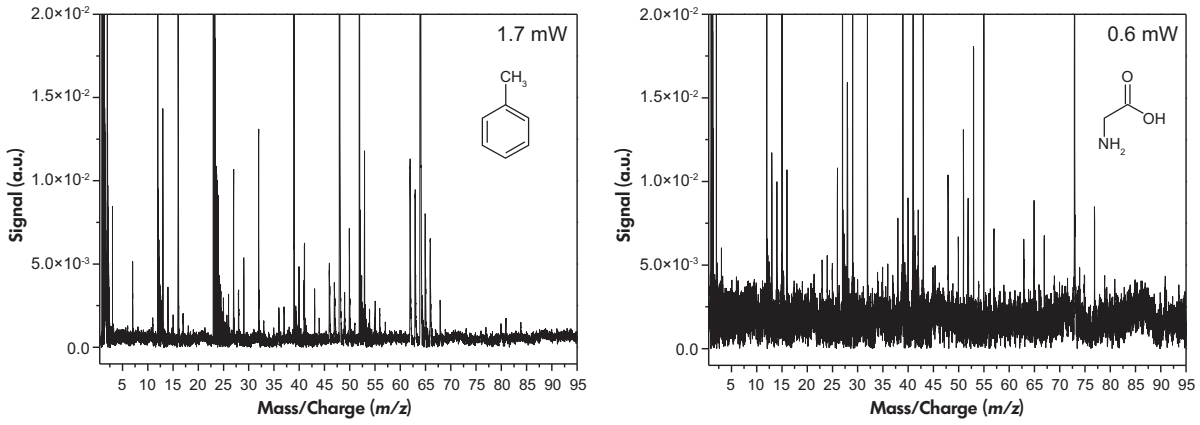

Figure 10. Laser desorption mass spectra of toluene film (left) and glycine film (right) obtained with the LMS equipped with the fs-laser desorption ion source. A complex fragmentation pattern was measured.

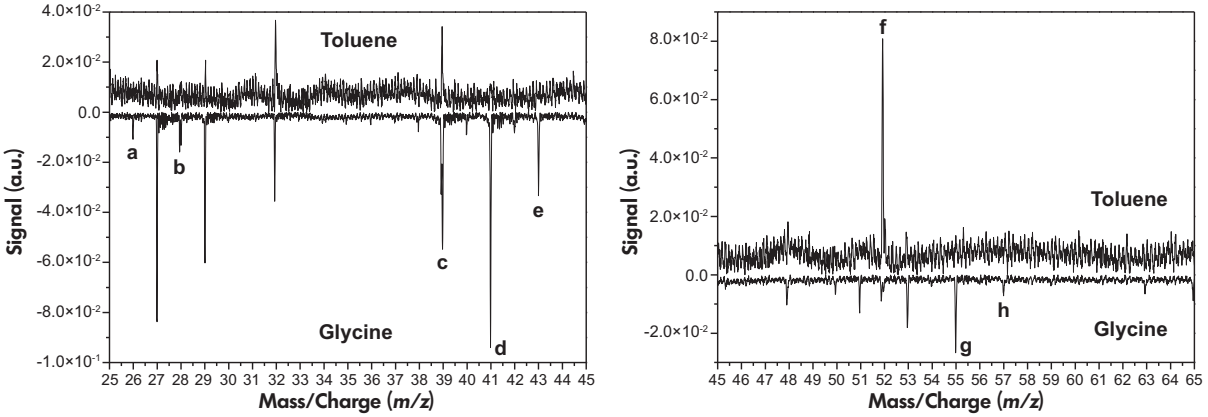

Figure 11. Comparison of selected mass regions of the toluene (upper trace) and glycine (bottom trace) mass spectra. Mass peaks a, b, d, e, g and h are characteristic only for glycine and they can be used to identify glycine or a glycine derivative from the other molecular compounds that are deposited on the surface. Further information on the assigned mass peaks can be found in Table 4.

Table 4.
Possible fragments for the assigned mass peaks shown in Fig. 11

Peak	Possible fragment	Mass	Peak	Possible fragment	Mass
a	CN	26	d*	C_2H_3N	41
a*	C_2H_2	26	e	C_2H_3O	43
b	CH_2N	28	f	C_4H_4	52
b*	CO	28	g	C_2HON	55
c	C_3H_3	39	h	C_2H_3ON	57
d	C_2HO	41	h*	C_2HO_2	57

needed to observe the desorption/ionisation product (Majer *et al.* 1981). A Coulombic explosion mechanism may explain the extended fragmentation for the laser desorption of glycine and toluene. Since the fs-laser couples well with electrons, surface charging effects and the degree of molecular ionisation can be high. Such multi-charged species can undergo Coulombic explosion easily, followed by formation of ionised small molecular species. For more detailed chemical analyses, investigations of various classes of molecular compounds have to be performed.

The laser desorption method applied here for chemical analysis is simple and thus applicable for *in situ* applications from a planetary rover or a lander. The laboratory methodology for the investigation of amino acids is well established and includes liquid chromatography coupled with postcolumn derivatisation (Rigas 2012) or coupling of chromatography with spray ionisation and mass spectrometry methods (Sakairi and Yergey 1991). Amino acids are also identified by their evaporation and electron ionisation of gaseous molecules via mass spectrometer and matrix-assisted laser desorption (MALDI) mass spectrometry (Kim *et al.* 2014). The application of these methods would be too risky with the current stage of technological development in space research. It would require a complex sample preparation phase, the application of sophisticated sample introduction systems or the application of more than one laser system (McSween *et al.* 2011).

Performance studies of MCS

The performance of MCS is comparable to that of the Beagle 2 microscope (Thomas *et al.* 2004). Because of progress in imaging technology, the current MCS is equipped with a more advanced sensor offering greater image resolution and dynamic range.

General features of MCS: MCS performs the optical characterisation of a solid sample, yielding the sample morphology. The camera system delivers fast multi-colour imaging by illuminating the sample with light of different wavelengths (blue: 480 nm, orange: 560 nm, red: 700 nm). MCS has a field of view (FOV) of 2 mm × 2 mm, a lateral resolution of 1 μm per pixel, and offers the possibility to

conduct polarisation analysis of the light reflected from the sample surface. It can be used also for surface fluorescence measurements after illumination of the surface by UV radiation (see Table 3, Lüthi 2008). Additional spectroscopic measurements can be performed by coupling the microscope with an IR emission analyser, which can be of considerable interest for the investigation of surface mineralogy with high spatial resolution.

Whether a region is in focus or not will determine the quality of imaging. MCS has a focal depth of ~ 40 μm (see Table 3). If the distance between any two surface points within the microscope's field is larger than about 40 μm, then parts of the image will appear smeared. With a sample size of ~ 1 mm, high-resolution imaging is possible at selected surface locations, although image stacking might be necessary. By taking a number of images, one can collect well-resolved surface regions while neglecting the remainder. The roughness of the surface can be deduced using this method by knowing the depth of focus.

Optical properties of a sample surface: Particle/grain size, texture and surface roughness of the material can be determined from optical and polarisation-controlled imagery. The lateral resolution is sufficiently high to resolve various surface components including individual micrometre-sized grains. In Figure 12, the capability of MCS to record high-resolution imagery of sample material is demonstrated; the structure in the basaltic volcanic rock is seen as irregular with dust grains deposited on the surface.

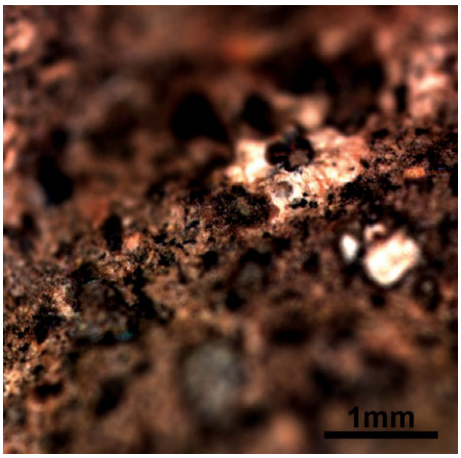

Figure 12. Image of mm-sized objects (impact melt rock with amygdales, Sääksjärvi Impact Crater, Finland) by the RGB illumination method performed by MCS. The high spatial resolution provides means for highly selective analyses of grain-sized objects. The image is not focused uniformly because of nonflat surface and the depth of field of the camera system.

The polarisation capabilities are helpful to reduce the effects from specular reflections and allow the analysis of the surface sharpness. The geometry of illumination conditions may affect colour ratio measurements of reflected light from the surface. Surface tilts can cause shadowing and colour variations originating from a non-uniform illumination of the surface. Other problems are introduced by specular reflections, which may dominate signal contributions from other illumination geometries. The effects can be analysed and eliminated if the sample geometry and illumination geometry are known (Lüthi 2008). Polarisation optics can be used to reduce these effects. An example of application of polarisation optics to reduce specular reflections is shown in Figure 13. This figure displays two images acquired using red light illumination with and without specular reflection. The shiny meteoritic surface produces specular reflections that dominate the image when polarising filters are not used. By combining a polariser and an analyser in the optical path, specular reflections can be eliminated and only the part of the light that underwent internal interactions with the sample and subsequently changed its polarisation state is investigated. The wavelength at which the analysis is carried out can be chosen according to the investigated target.

An insight into local particle surface mineralogy can be gained by analysis of the images taken in four different colours (blue, orange, red and NIR). Multi-colour image analyses allow spectral diagnosis of the sample surface and an insight into regolith type and processes contributing to the formation or modification of the surface material (Vilas *et al.* 1994). Analysis of the inter-relation between minerals and investigation of mineral composition at grain level is of considerable interest because of the mineralogical context (Neuland *et al.* 2014). Illumination of the sample with UV light can also be useful, for example for fluorescing minerals (see Figure 14 for example images). The surface fluorescence imaging capability and imagery of the surface in polarised light can be also useful in surface diagnostics for the presence of organic or bio-organic deposits. Bio-organic material deposited on sample surfaces can be clearly distinguished by comparing multi-colour and fluorescence images (see investigations on sample 194HS435; Pullan 2008, Pullan *et al.* 2008).

Studies on a graphitic sample by LMS and MCS

The graphite sample used in this study is a natural rock sample collected from the 'Los Pobres' graphite mine, Spain

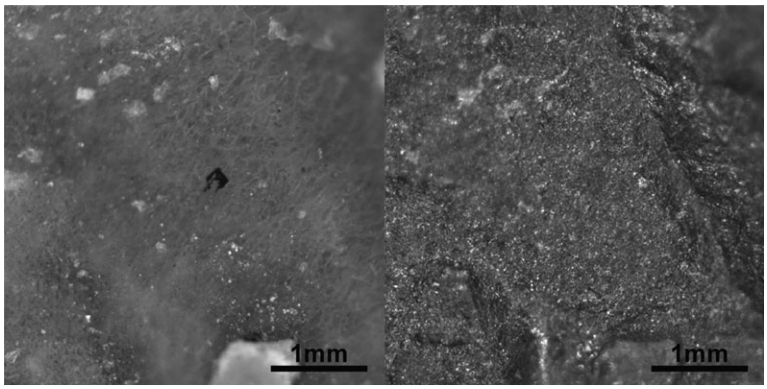

Figure 13. Microscope images using red light-emitting diodes. The left image was measured with polarisation control by registering the light reflected internally (changed polarisation state) while the right image shows solely the specular reflections (unchanged polarisation state).

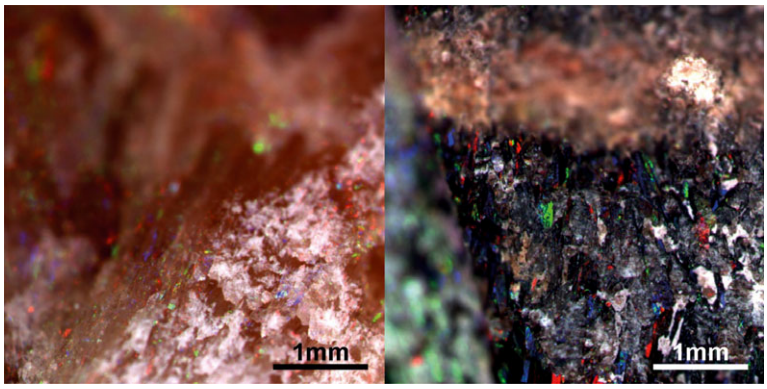

Figure 14. Examples of images of surface fluorescence recorded after surface irradiation by UV light. Left: calcite from karst in gypsum (Krattigen gypsum mine, Switzerland); Right: Black calcite fluorescence limestone (Keuper, Heubhof, SH, Switzerland).

(see Figure 3, left panel). It consists of graphite inclusions between two silicate host rock phases (Ronda sample). The optical and mineralogical characterisation of both graphitic inclusions and host rock phase were conducted using MCS and LMS to provide the chemical (element/isotope) composition of selected surface areas of the sample.

Host rock surface characterisation

MCS analysis: Imagery of an arbitrarily selected area on the graphite sample (see *Samples and reference materials*, above) was measured using illumination by RGB light. A composite image was made by combining the three-colour images. Figure 15 displays images of the host rock surface structure, whereas Figure 16 shows a section where the laser ablation mass spectrometric analyses were conducted (the laser ablation craters are seen as dark spots). The sample consists of serpentinised peridotite and graphite, and a rich mineralogical composition is expected. Striations and slickensides are common features seen in these rocks indicating the effect of tectonic faulting or shearing.

Because of its serpentine composition, the surface is expected to reveal predominantly O, Si, Fe and Mg. In addition, a few trace elements including Ni, As and Cr can be detected (Luque *et al.* 1992, Crespo *et al.* 2006). The ablation craters have elliptical outlines (approximate dimensions 20 μm × 10 μm) and were separated by about 70 μm from each other (centre to centre, see close-up in Figure 15a). For each of the locations, mass spectrometric information was gathered. There is no evidence for the presence of ablation rims or material redistribution around the ablation pits (Figure 16).

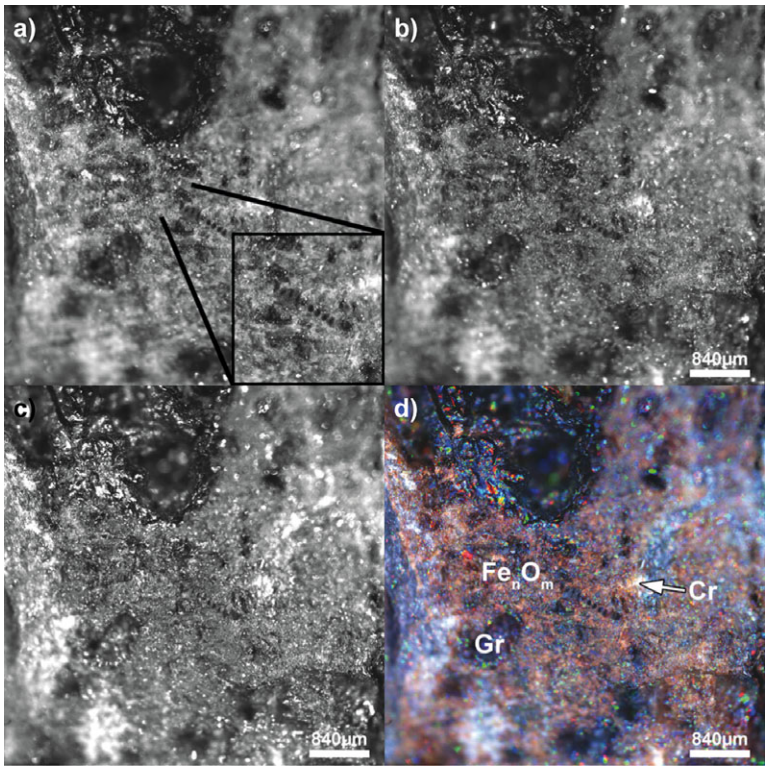

Figure 15. Images of the Ronda sample taken with RGB illumination in which (a) represents red, (b) green and (c) blue. The composite image of the host rock is represented by (d) and where Cr = iron-rich chromite, Gr = pure graphite crystals and Fe_nO_m = iron oxides (in serpentine). The sharpness of the image could be maintained in the central image area. In panel (a), a close-up of the craters is shown.

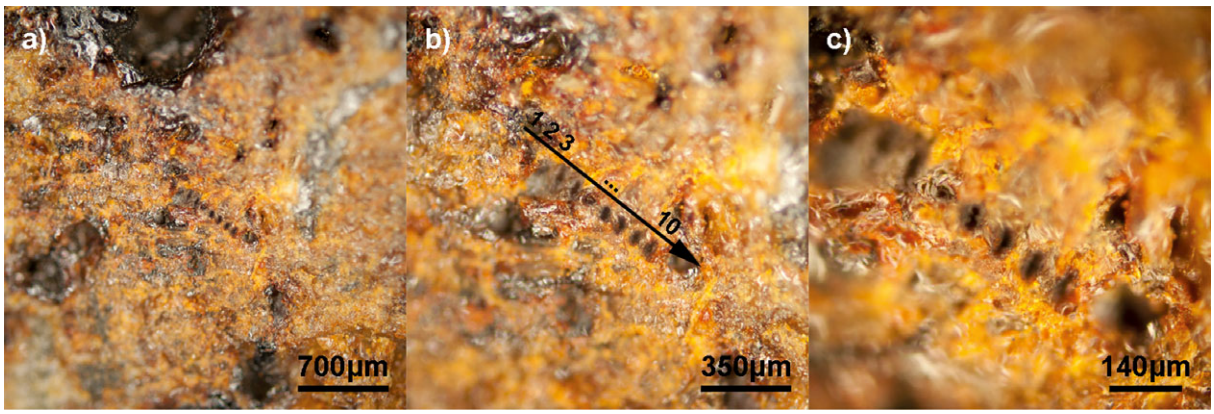

Figure 16. Expanded section of Figure 15 (serpentine-rich host rock) showing the surface locations investigated by laser mass spectrometry on the Ronda sample. Ten different sample locations were analysed, as seen by the craters with dimensions of about 20 µm × 10 µm. These images were captured with a commercial microscope equipped with a camera system. Black/dark grey colour is representative of graphite and yellowish colour of iron oxide-rich serpentine.

LMS analysis: Typical laser ablation mass spectra (LG and HG channels) of the Ronda sample, which were recorded for the host rock region in the graphite sample, are shown in Figure 17. Only the mass region where major elements were measured is shown in the figure. The LG channel spectrum (Figure 17 upper panel) depicts elements with concentrations larger than a few hundred ppm. Several mass peaks assigned to clusters (i.e., multi-atom

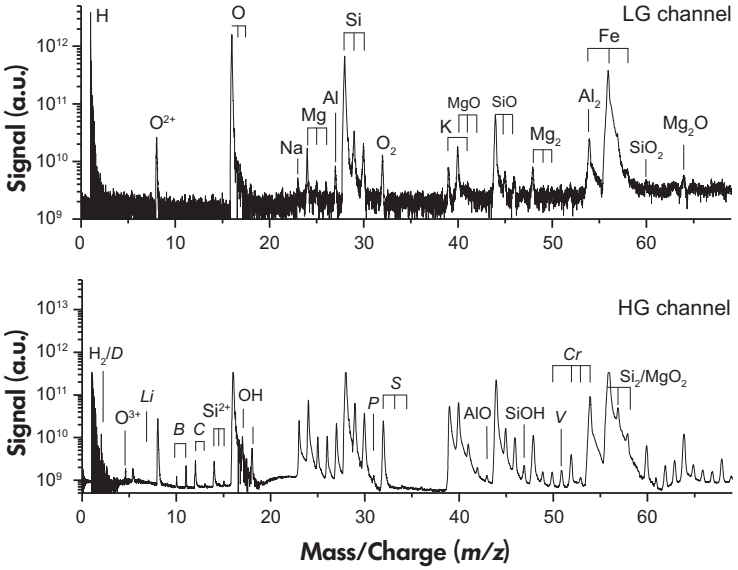

Figure 17. Typical low-gain (LG) and high-gain (HG) channel mass spectra of the host rock phase of the graphite sample (Ronda sample). The LG channel spectrum delivered detection of elements with concentrations larger than a few hundreds of ppm and shows major elements detected in the sample. In the HG channel, spectrum elements with concentrations down to a few ppm were detected.

ions) and oxides were also identified in the spectrum (O_2, MgO, SiO, Mg_2, SiO_2). These were probably produced by recombination of major elements during the laser plume expansion rather than ablated directly from the sample surface. Direct desorption of the clusters is highly unlikely under the applied laser ablation ion source condition (high laser irradiance). As expected for the host rock phase, O, Si, Fe, and Mg are the major elements identified in the spectra and the assignment is presented directly in the mass spectrum plot. The assignment is supported by identification of their isotope patterns. The isotope ratios determined from the mass spectrometric analysis of the main elements are typically close to their terrestrial isotope ratios, and accuracy of the analysis is typically a few per mil (Figure 18). Occasionally, larger discrepancies in measured isotope ratios to those of terrestrial values were observed for Fe because of isotopic interference by ^{54}Cr, silicon dimer (Si_2) and/or magnesium dioxide (MgO_2) with the Fe isotopes of mass 54, 56 and 57. The detection sensitivity in the HG channel was substantially larger compared with the LG channel by design. However, the increase in the sensitivity in this channel occurs here at the expense of saturation of the most intense peaks in the spectrum. To achieve a high effective dynamic range for the measurements, they were cross-calibrated.

Only non-saturated mass peaks were used for cross-calibration between the LG and HG channels. In the present study, isotope mass peaks ^{25}Mg, ^{26}Mg and ^{29}Si, ^{30}Si and ^{27}Al were selected for cross-calibration. Taking into account the effective dynamic range of the LG and HG spectra and the scaling factor of about 100, elements with concentrations down to sub-ppm could be measured by LMS. The mass spectrum recorded in the HG channel is presented in the bottom panel in Figure 17. In addition to major elements, several minor and trace elements were detected in the sample. The mass peaks assigned to these elements are shown in Figure 17 as well as less abundant clusters formed in the ablation process.

For the detection of minor and trace elements and determination of their concentration, careful calculation of isotope composition of interfering clusters often has to be taken into account to evaluate their contribution to the intensity of a particular mass peak. An isotope normalisation procedure was applied assuming terrestrial isotopic abundance for determination of element abundance. Figure 18 displays the results of isotope determination of several major elements from the mass spectrum measured at location 1. The green bars without black borders correspond to isotopes with terrestrial abundances used for the isotope determination, whereas the green bars with black borders correspond to isotopes with terrestrial abundances not used for analysis; the bars in yellow denote the calculated abundance of the specific isotope used for analysis. The accuracy of the isotope ratio for major elements is expected to be at the per mil level, and larger discrepancies indicate either a contribution from isobaric clusters or an isotope of another element. The

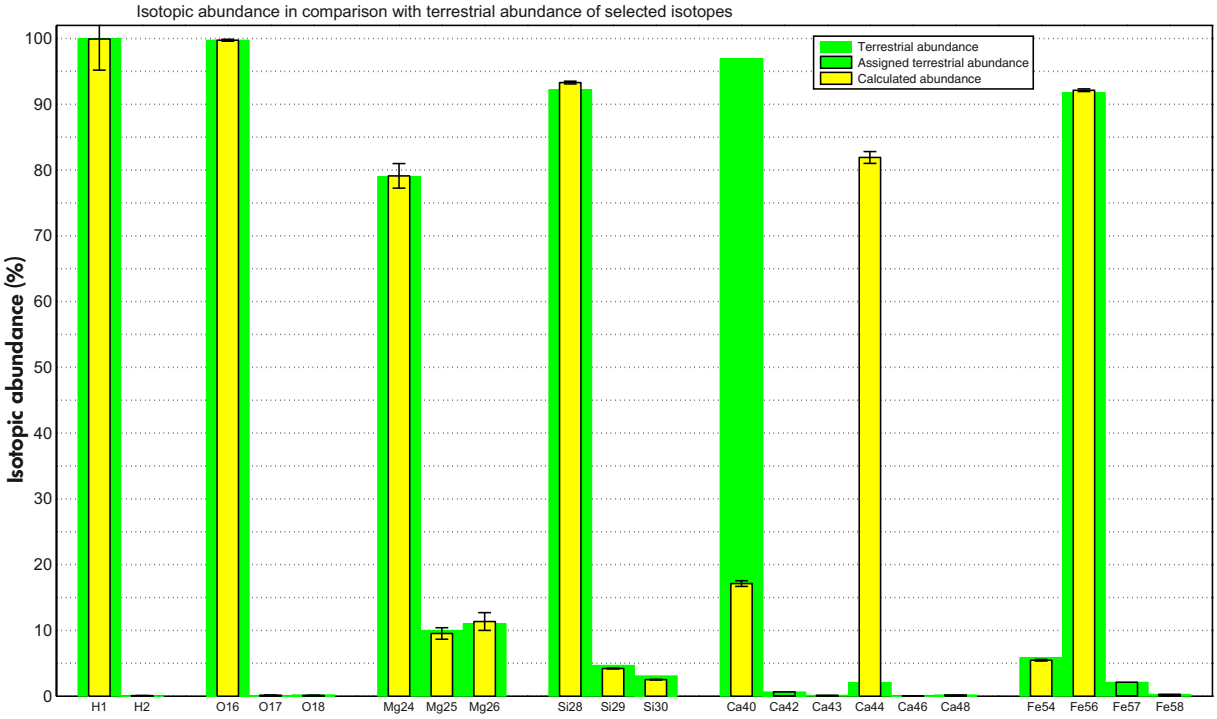

Figure 18. Histograms of isotope ratios for major elements contained in the host rock of the graphite sample. The isotope ratios of major elements could be determined with accuracy at the per mil level. In case of discrepancies, a contribution from isobaric masses is to be suspected (isotope components of another element, or cluster). The isotopic mass peak components of Ca, Cr and Fe can interfere with mass peaks of MgO (*m* = 40, 41, 42 amu), SiO (*m* = 44, 45, 46 amu) and AlO (*m* = 43 amu); Mg_2 (*m* = 48, 49, 50 amu), Al_2 (*m* = 54 amu), Si_2 (*m* = 56, 57, 58 amu) clusters can make the quantitative analysis in the relevant mass ranges difficult.

measurements of Ca, Ti, V, Cr and Mn can be difficult if contributions from MgO, AlO, SiO or Mg_2, and Al_2 are large. The concentrations of the major and trace elements that were identified for the ten measured locations are presented in Table 5. The concentrations of Li, B and P were determined in the range 0.1–10 ppm and C, S, Ca, Ti, V, Mn, Cr and As as 10–100 ppm. Sodium, K and Li could be either present in the sample or as terrestrial contamination of the sample surface. The depth profiling analysis showed that the concentration of these elements reduces substantially

Table 5.
Atomic fractions of the main elements detected in the host rock phase of the graphite sample

Measurement location	Concentrations of major elements in atomic fractions in the Ronda sample (%)				
	O	Mg	Al	Si	Fe
1	48.7 (0.3)	0.5 (0.1)	0.2 (4.2)	25.3 (0.2)	25.3 (0.3)
2	44.5 (0.3)	0.7 (0.1)	0.3 (4.3)	27.3 (0.1)	27.3 (0.4)
3	32.1 (0.2)	1.1 (0.05)	0.3 (4.0)	33.2 (0.3)	33.2 (0.3)
4	44.0 (0.3)	0.1 (0.02)	0.4 (1.7)	27.7 (0.4)	27.7 (0.3)
5	0.1 (0.05)	5.8 (0.3)	1.3 (1.1)	46.4 (0.5)	46.4 (0.4)
6	52.5 (0.5)	0.8 (0.3)	0.4 (5.2)	23.2 (0.3)	23.2 (0.2)
7	58.3 (0.3)	2.9 (0.2)	0.3 (2.8)	19.3 (0.4)	19.3 (0.3)
8	61.9 (0.2)	0.5 (0.1)	0.1 (8.7)	18.8 (0.3)	18.8 (0.3)
9	61.6 (0.4)	0.04 (0.01)	0.2 (2.5)	19.1 (0.2)	19.1 (0.3)
10	43.9 (0.3)	1.0 (1.7)	0.3 (2.1)	27.4 (0.3)	27.4 (0.3)

Li, B and P: 0.1–10 ppm; C, S, Ca, Ti, V, Mn, Cr and As: 10–100 ppm. The errors (in brackets) of the determined atomic fraction do not exceed a few per cent of the measured value.

after removing the uppermost 5–10 μm of the sample surface. This was achieved after the first 10000 laser shots. Table 5 lists the measured abundance of the major elements for each of the ten investigated sample locations.

The RSCs of the main elements were assumed to be close to one, which is consistent with the results of our earlier analysis of NIST SRM samples. Hence, concentration values obtained directly in the mass spectrometric analysis were taken without further corrections. Uncertainty of the determined concentration values due to the consumption of elements to produce clusters was not taken into account.

Graphite sample surface

The graphitic accretions, found within the serpentinitic host rock, consist of various phases formed at different temperatures and include amorphous and crystalline phases of graphite. The amorphous phase is predicted to have a lower temperature of formation compared with the crystalline graphite. The latter has a crystallisation temperature around 800 °C and a magmatic origin. The crystalline phase is crystalline because the temperature of graphite formation is close to the graphite precipitation temperature, whereas the amorphous phase could have been the result of a rapid cooling of the melt and, thus, precipitation of the graphite was too fast to have sufficient time for crystallisation. The entire sample of the graphite can also contain mineral inclusions. The studies conducted on the graphite surface aimed to identify these phases with the help of microscope imagery (optical properties) and element composition.

MCS analysis: In Figure 19, three-colour illuminated images (RGB, a, b, c) and a derived composite image (d) of the graphite sample surface are shown. An expanded view of the analysis region is presented in Figure 20.

The laser ablation craters are readily observed (Figures 19 and 20). Again, no melting rims or any material redistribution around the crater were observed. Despite the fact that no changes to the experimental set-up were made during these two experiments, contrary to previous images (Figures 15 and 16), the crater structure is clearly circular, whereas in the previous images of the host rock phase, an

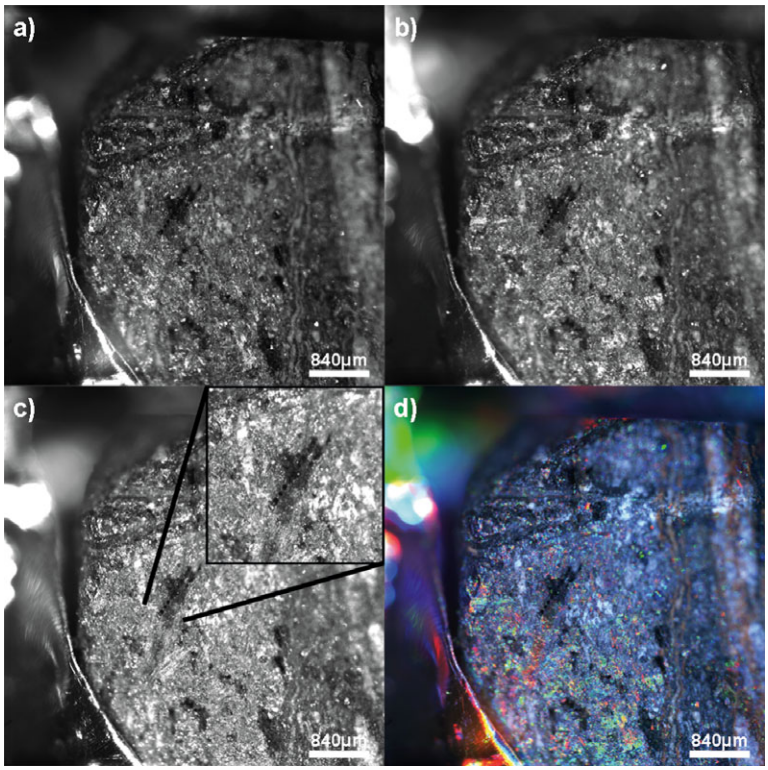

Figure 19. Three-colour illumination images (RGB, a, b, c) of the Ronda sample and derived composite (d) image of the region of the pure graphite surface investigated by MCS and laser mass spectrometry. Close-up view in the third image (c) shows a number of laser ablation craters, which were formed during mass spectrometric measurements. The small white dots represent inclusions of relatively pure iron-rich chromite. The black colours represent mineral inclusions containing chromite and iron oxides (d).

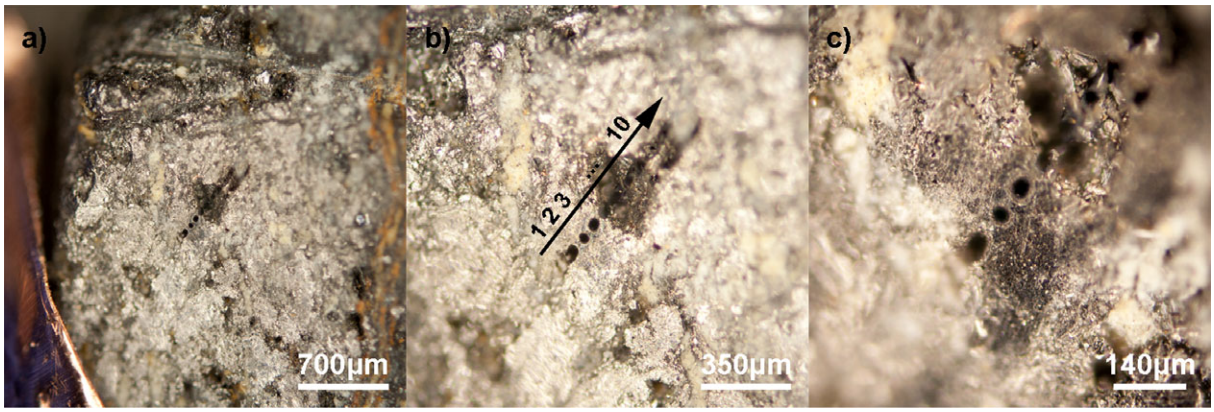

Figure 20. Expanded section of the graphitic surface of the Ronda sample showing the craters formed during the laser ablation mass spectrometric investigations. A rounded crater shape with the crater diameter of about 17 µm could be determined from the image analysis. These images were recorded with a commercial laboratory microscope system equipped with a camera system.

asymmetric crater shape was observed. (The circular shape of the crater in graphite may be because it is a soft, homogenous material and thus, the ablation rate was relatively constant across the ablated surface.) From these images alone (Figures 19 and 20), it is challenging to say whether the laser ablation studies were performed within the crystalline or the amorphous phase. Nevertheless, it seems that measurement locations 1 and 4 (as labelled in Figure 20b) were situated on the graphitic phase and location 2, possibly, mainly sampled crystalline graphite. Nevertheless, the second crater may also cover both crystalline and amorphous phases since the graphite crystals are often only a few micrometres in size. This means that the corresponding mass spectrum should show mostly pure carbon and no oxygen or other trace elements. Crater number 4 is close to a small cavity. Craters 5–8 are located on a mineral inclusion, and their element composition is probably comparable to that of the host rock. Finally, ablation craters 9 and 10 are seen to be located in the graphitic phase.

LMS analysis: Ten laser ablation mass spectrometric investigations were made across the graphite surface (Figure 20). A typical mass spectrum is dominated by an intense mass peak of C and moderately intense mass peaks of O, Mg, Al, Si and Fe. Furthermore, the mass spectrum shows the presence of carbon clusters extending in range up to about 400 amu ($C–C_{24}$) as well as oxides of carbon (oxocarbon) where oxygen abundance at the sampling location was sufficiently high. Hence, carbon clusters formed readily in the expanding plasma plume that was formed during the laser ablation process and can complicate mass spectrometric analysis. The mass spectra recorded in the LG and HG channels are presented in Figure 21.

Figure 22 shows an overview of LG channel mass spectra for a few investigated sample locations. The mass spectrum measured at location 4 (Ronda 4) contains mainly mass peaks of carbon and carbon clusters and, due to the absence of oxygen, is expected to be a crystalline carbon spectrum. Trace elements measured at this location are Mg, Si, Al and Fe. In the mass spectrum recorded at location 3 (Ronda 3), C was the major element and O, Mg, Si, Al and Fe were identified at minor/trace levels. Similar spectra were recorded at locations 1, 2, 5, 9 and 10. The oxygen concentration determined from each of these locations was variable. The chemical composition of a mineral inclusion (locations 6, 7 and 8) contained mainly Al, Mg and O with minor concentrations of the metallic elements Ti, V, Cr, Fe and Mn. The concentrations of major and minor elements determined from these ten locations are given in Table 6. For the calculations of atomic concentrations of Mg, Cr and Fe, the mass peaks of ^{26}Mg, ^{53}Cr and ^{57}Fe isotope components were selected and the values obtained by these analyses were cross-checked with the results obtained from other isotope components. Also, the contributions from clusters, for example C_2, CH, C_4, Al_2, MgO_2, Si_2, were carefully evaluated. The assignment of elements and C-clusters is presented in Figure 22 and is supported by the analysis of their isotope structure. The isotope ratios of C, O and Si were close to their terrestrial values within per mil accuracy, but Mg isotope ratios were affected by a C_2 peak at 24 amu (Figure 20). For Mg, Cr and Fe, isotope ratios varied by a few per cent, again indicating interference by clusters.

Variation of C and O concentrations could be used for identification of the graphite phases. While the crystalline

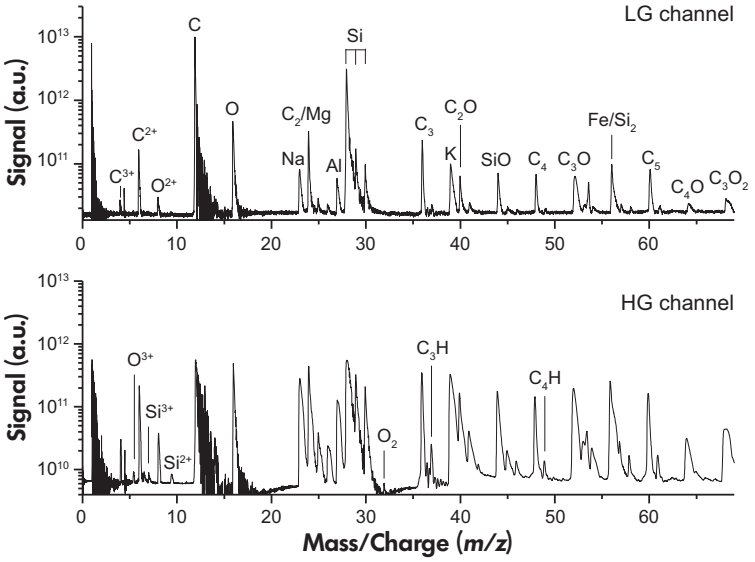

Figure 21. Mass spectra of the amorphous graphitic sample (Ronda sample) recorded in low-gain and high-gain channels with the assignment recorded at crater 1 (Figure 20, panel b). Very similar spectra were obtained at other locations. The mass spectrum was dominated by intense peaks of C and O and their oxocarbon compounds. The main elements (Mg, Al, Si and Fe) detected in the host rock surface were identified in graphitic material at much lower concentrations compared with C concentration. The spectrum shows a long progression of mass peaks characteristic of carbon- and oxocarbon-clusters.

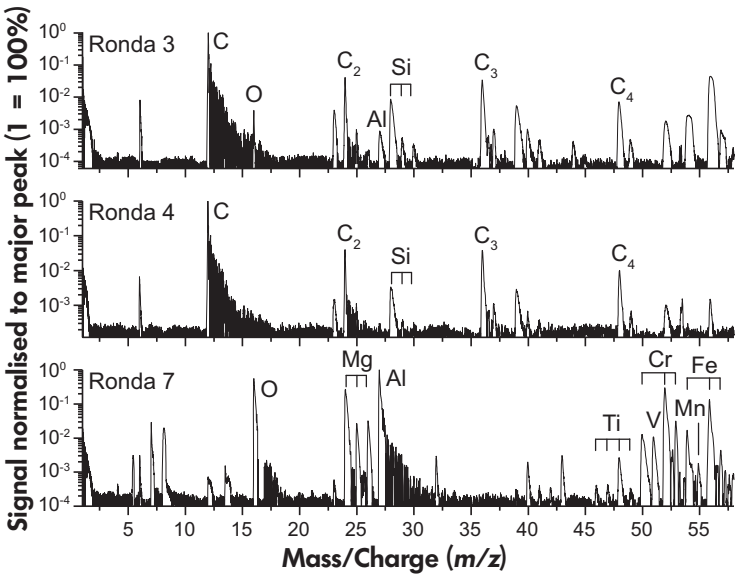

Figure 22. Overview of mass spectra of the Ronda sample recorded in the low-gain channel at locations 3, 4 and 7. The mass spectrum of location 3 is similar to that recorded at locations 1, 2, 5, 9 and 10. At location 4, no O was detected and the spectrum shows mainly mass peaks of C and carbon clusters. The mass spectrum recorded at location 7 is similar to that measured at locations 6 and 8. Mineral inclusions contained mainly O, Mg and Al with admixtures of several metallic elements.

graphite is expected to contain no oxygen, in the amorphous phase, oxygen could be detected. At measurement locations 1–3, 9 and 10, probable mixtures of amorphous and crystalline graphitic phases were detected, whereas very likely pure crystalline graphite was measured at location 4 where no oxygen was found and substantially

Table 6.
Concentrations of the main elements determined from the mass spectrometric analysis of the graphite sample (Ronda sample) at ten different locations

Location	Concentration of main elements in atomic per cent fraction [%]						
	C	O	Mg	Al	Si	Cr	Fe
1	46.56 (1.0)	6.53 (0.4)	0.62 (0.08)	3.27 (0.3)	38.85 (0.2)	0.19 (0.19)	3.97 (0.2)
2	59.60 (0.7)	0.31 (0.06)	0.05 (0.03)	2.66 (0.1)	11.75 (0.4)	1.85 (0.1)	23.78 (0.9)
3	85.08 (0.6)	0.23 (0.08)	0.28 (0.05)	0.29 (0.03)	3.34 (0.1)	0.11 (0.03)	10.67 (0.2)
4	84.41 (1.3)	0.004 (0.003)	0.026 (0.07)	0.039 (0.011)	3.10 (0.3)	4.62 (0.2)	7.80 (0.2)
5	26.25 (0.7)	3.00 (0.15)	3.33 (0.01)	13.81 (0.3)	0.64 (0.2)	3.54 (0.1)	49.42 (0.2)
6	0.81 (0.2)	0.04 (0.02)	3.18 (0.02)	3.72 (0.2)	0.059 (1.1)	56.42 (0.1)	35.76 (0.5)
7	0.59 (0.22)	0.11 (0.04)	0.15 (0.02)	0.60 (0.3)	0.27 (0.3)	67.92 (0.1)	30.35 (0.5)
8	0.028 (0.2)	0.15 (0.03)	0.12 (0.03)	0.59 (0.3)	0.15 (1.0)	78.07 (0.19)	20.89 (0.6)
9	37.70 (0.3)	10.17 (0.01)	1.46 (0.09)	1.03 (2.9)	46.51 (0.1)	0.49 (0.9)	2.64 (0.2)
10	58.27 (0.2)	1.19 (0.05)	1.38 (0.03)	3.47 (0.2)	32.61 (0.1)	0.54 (0.2)	2.53 (0.2)

Uncertainties are given in parenthesis.

lower concentrations of host rock elements were measured. At location 5, a transition between graphitic and rock phases was observed. At locations 6–8, mineral inclusions were identified with relatively high concentrations of Mg, Cr and Al and a moderate fraction of Si and other metallic elements including Ti, V, Cr and Fe. These can be seen in the overview mass spectra (Figure 22, Ronda 7).

More advanced investigations of these two phases are planned. Application of smaller laser ablation spots can be helpful for investigation of individual crystalline graphite samples. Further determination of C and O isotope structure is also desirable to deepen our knowledge of the formation processes of the two graphite phases.

Design of the CAMAM analytical suite

A miniature instrument suite CAMAM, which combines MCS, LMS and a sample collecting and introduction system (SCIS) was proposed for ESA's MarcoPolo-R mission to an asteroid (http://sci.esa.int/marcopolo-r). The CAMAM analytical suite is an ensemble of four hardware systems: (i) the laser mass spectrometer (LMS), (ii) the MCS, (iii) a SCIS and (iv) an electronics box (E-Box). The four systems were assembled and tested individually at subsystem level. Once all four subsystems were tested, they could be integrated easily into the complete CAMAM instrument suite. Due to the highly integrated design, the qualification and acceptance of environmental tests were carried out at instrument level. The CAMAM instrument suite has direct flight heritage from earlier space missions (Mars Express, Thomas *et al.* 2004 and Rosetta, Thomas *et al.* 1998, Balsiger *et al.* 2007). The lightweight design was optimised for compactness and employed simple interfaces (see Table 7).

Table 7.
Mass and power consumption of the CAMAM instrument suite

Quantity	Value
Dimensions [*x*, *y*, *z*]	310 mm × 227 mm × 272 mm
Mass	
Basic mass	4 kg
Margin	20.0%
Nominal mass including margin	4.8 kg
Power	
Standby power of analytical suite	6.6 W
Peak power	17.7 W
Average power	9.9 W
Margin average power	20.0%
Average power incl. margin	11.9 W

Figure 23 shows the schematics of the CAMAM instrument suite with its four subsystems. The laser mass spectrometer and the microscope-camera were mounted isostatically to a common optical bench, which was made of a near-zero-CTE carbon fibre composite. Both the MCS and LMS sensors were aligned to provide complementary measurements of the same location. Depending on the space mission, that is whether CAMAM is placed in an orbiting spacecraft, a lander or a rover, SCIS has to be designed and realised differently. In Figure 23, a SCIS design is shown that was prepared for the MarcoPolo-R space mission – a mission to land on an asteroid. In this case, samples are collected with an electrically polarised metal band, deployed outside the instrument enclosure. By retracting the band, the collected dust grains are brought in the field of view of the MCS and LMS. Two guide wheels, which are directly attached to the first (extraction) electrode, ensure that the samples are within the focus depth of the instrument. Appropriate material choice for the realisation of the sensor components guarantees the compensation of the different thermal expansions and eliminates the need of

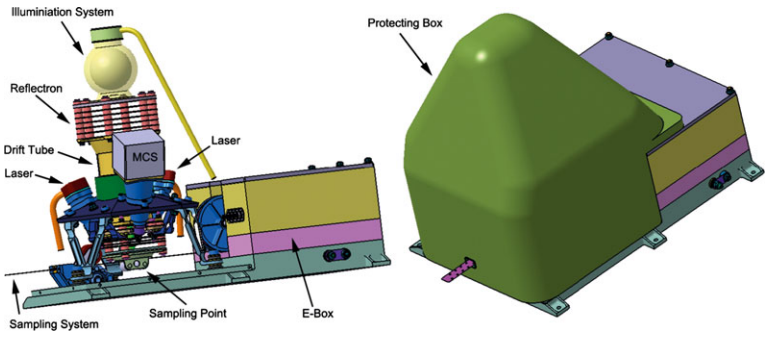

Figure 23. Left: Schematic diagram of the CAMAM instrument suite. LMS and MCS are aligned to allow for complementary measurements of the same sampling point. A sample is delivered to the sampling point by a sample introduction system; here, a particle trap mechanism is shown. The electronic systems are located in the E-box. Right: The instrument suite with its protective cover.

an additional system supporting optimal focusing of the laser on the sample and positioning of MCS for optimal imaging of the sample. The sample illumination hardware for MCS is mounted to the backplane of the reflectron of LMS (Figure 23).

A lightweight glass-fibre enclosure (protecting box, Figure 23) prevents the exposure of high voltages to the environment and protects the Sensor Unit against mechanical damage and contamination from the environment. The electronics are arranged in a vertical stack of discrete modules. All internal connections are covered by the protective enclosure.

High sensitivity and accurate mass spectrometric analysis coupled with high-resolution optical imaging and spectroscopy of surface composition is a powerful and fast method for the investigation of complex inhomogeneous materials in an extraterrestrial environment. The combination of LMS and MCS will deliver full chemical analysis including mineralogical surface context and morphological surface details, both with micrometric spatial resolution allowing fast, selective and sensitive analyses of surface details down to µm-sized grains. Chemical surface mapping, with a lateral resolution of micrometres, combined with vertical chemical analysis of the surface and subsurface of samples should provide a wide array of information on chemical and physical processes, necessary for a better understanding of the origin and evolution of the material. With the latter capabilities, several important analyses can be performed, including geochronology of extraterrestrial material by radiogenic isotope methods, evaluation of uppermost surface layer modification by space weathering, aqueous alteration processes or investigation of possible surficial organic deposits. The performance of both MCS and LMS sensors is exceptional, and together, they have the potential to deliver information on chemical and physical properties of a sample with sensitivity, accuracy and precision close to that of laboratory counterparts. Both instruments can be used for the detection of molecular species deposited on the surface of materials.

Summary

Two miniature instruments, a laser ablation/ionisation mass analyser (LMS) and a microscope-camera system (MCS), were developed for *in situ* investigation of planetary materials. In the present investigation, their performance and capability to conduct morphological, mineralogical and chemical investigations of rock or regolith/soil samples were demonstrated. Optical analysis leads to visualisation of the morphology of sample surfaces and provides clues as to the mineralogical composition. With the help of MCS, the chemical composition of the sample surface at several well-defined locations could be investigated by laser ablation mass spectrometry. The element and isotope composition could be delivered from the mass spectrometric analysis to constrain mineralogical context by means of major element composition. Additionally, trace elements with concentrations below the ppm abundance level were measured. Isotope ratio analysis was performed with accuracies at the per mil level for all major elements, helping in the assignment of the element spectra in the case of isobaric interference from molecular clusters. The accuracy of the isotope ratio measurements was sufficiently high to investigate isotopic fractionation of low atomic number elements. This is of importance in the investigation of formation processes and determination of the conditions at which materials were formed.

MCS and LMS are thought to be very useful in conducting the *in situ* analysis of planetary soils if combined

in a miniature instrument suite, CAMAM. Such an instrument suite has the potential to open new perspectives in space research. Applying complementary methods (high-resolution optical imagery and sensitive mass spectrometry) to investigate the same surface of samples with sizes down to micrometres allows the detailed characterisation of physical and chemical properties of planetary solids. CAMAM combines two sensor techniques which, until now, have been applied in space research as standalone instruments, and has a heritage in a number of past and current space missions, and laboratory and field experiments.

Acknowledgements

The authors thank the Swiss National Science Foundation for continuing support. All members of the CAMAM team are thanked for their input in the preparation of the instrument design for MarcoPolo-R Mission. Alain Péteut is thanked for the help in preparation of MCS instrument for the current studies. Funding provided from the Swedish National Space Board (project contract no. 100/13), and the Swedish Research Council (Contract no. 2012-4364) is acknowledged.

References

Balsiger H., Altwegg K., Bochsler P., Eberhardt P., Fischer J. and forty-five others. (2007)
ROSINA–Rosetta orbiter spectrometer for ion and neutral analysis. Space Science Reviews, 128, 745–801.

Brinckerhoff W.B., Managadze G.G., McEntire R.W., Cheng A.F. and Green W.J. (2000)
Laser time-of-flight mass spectrometry for space. Review of Scientific Instruments, 71, 536–545.

Campbell J.L., Perrett G.M., Gellert R., Andrushenko S.M., Boyd N.I., Maxwell J.A., King P.L. and Schofield C.D.M. (2012)
Calibration of the Mars science laboratory alpha particle X-ray spectrometer. Space Science Reviews, 170, 319–340.

Chicarro A., Martin P. and Trautner R. (2003)
The Mars Express mission: An overview. ESA SP, 1240, 1–11.

Cousin A., Forni A., Maurice S., Gasnault O., Fabre C., Sautter V., Wiens R.C. and Mazoyer J. (2011)
Laser induced breakdown spectroscopy library for the Martian environment. Spectrochimica Acta Part B, 66, 805–814.

Cousin A., Sautter V., Fabre C., Maurice S. and Wiens R.C. (2012)
Textural and modal analyses of picritic basalts with ChemCam laser-induced breakdown spectroscopy. Journal of Geophysical Research – Planets, 117, 1–9.

Cremers D.A. and Chinni R.C. (2009)
Laser-induced breakdown spectroscopy – Capabilities and limitations. Applied Spectroscopy Review, 44, 457–506.

Crespo E., Luque F.J., Rodas M., Wada H. and Gervilla F. (2006)
Graphite–sulfide deposits in Ronda and Beni Bousera peridotites (Spain and Morocco) and the origin of carbon in mantle-derived rocks. Gondwana Research, 9, 279–290.

Cui Y., Bhardwaj Ch., Milasinovic S., Carlson R.P., Gordon R.J. and Hanley L. (2013)
Molecular imaging and depth profiling of biomaterials interfaces by femtosecond laser desorption post-ionization mass spectrometry. Applied Materials and Interfaces, 5, 9269–9275.

Friend C.M. and Muetterties E.L. (1981)
Coordination chemistry of metal surfaces. 3. Benzene and toluene interactions with nickel surfaces. Journal of the American Chemical Society, 103, 773–779.

Grotzinger J.P., Crisp J., Vasavada A.R., Anderson R.C., Baker C.J., Barry R., Blake D.F., Conrad P., Edgett K.S., Ferdowski B., Gellert R., Gilbert J.B., Golombek M., Gomez-Elvira J., Hassler D.M., Jandura L., Litvak M., Mahaffy P., Maki J., Meyer M., Malin M.C., Mitrofanov I., Simmonds J.J., Vaniman D., Welch R.V. and Wiens R.C. (2012)
Mars science laboratory mission and science investigation. Space Science Reviews, 170, 5–56.

Herkenhoff K.E., Squyres S.W., Bell J.F., Maki J.N., Arneson H.M., Bertelsen P., Brown D.I., Collins S.A., Dingizian A., Elliott S.T., Goetz W., Hagerott E.C., Hayes A.G., Johnson M.J., Kirk R.L., McLennan S., Morris R.V., Scherr L.M., Schwochert M.A., Shiraishi L.R., Smith G.H., Soderblom L.A., Sohl-Dickstein J.N. and Wadsworth M.V. (2003)
Athena microscopic imager investigation. Journal of Geophysical Research – Planets, 108, 1–23.

Herkenhoff K.E., Grotzinger J., Knoll A.H., McLennan S.M., Weitz C. and forty-four others. (2008)
Surface processes recorded by rocks and soils on Meridiani Planum, Mars: Microscopic imager observations during Opportunity's first three extended missions. Journal of Geophysical Research – Planets, 113, 1–39.

Hillenkamp F. (1982)
Laser desorption techniques of non-volatile organic-substances. International Journal of Mass Spectrometry and Ion Processes, 45, 305–313.

Khartov V.V., Zelenyi L.M., Dolgopolov V.P., Efanov V.V., Zaytseva O.N., Lukiyanchikov A.V., Martynov M.B. and Pichkhadze K.M. (2011)
New Russian lunar unmanned space complexes. Solar System Research, 45, 690–696.

Kibler L.A. (2003)
Preparation and characterisation of noble metal single crystal electrodes. Monograph for the International Society of Electrochemistry, 55pp.

Kim K.J. and Hasebe N. (2012)
Nuclear planetology: Especially concerning the Moon and Mars. Research in Astronomy and Astrophysics, 12, 1313–1380.

references

Kim J.-I., Park J.-M., Kang M.J. and Pyun J.-C. (2014)
Parylene-matrix chip for small molecule analysis using matrix-assisted laser desorption/ionisation time-of-flight mass spectrometry. Rapid Communication in Mass Spectrometry, 28, 274–280.

Li X., Brinckerhoff W.B., Managadze G.G., Pugel D.E., Corrigan C.M. and Doty J.H. (2012)
Laser ablation mass spectrometer (LAMS) as a standoff analyzer in space missions for airless body. International Journal of Mass Spectrometry, 323–324, 63–67.

Libuda J. and Scoles G. (2000)
Collision-induced desorption of hydrocarbons physisorbed on Au(III). Journal of Chemical Physics, 112, 1522–1530.

Lin Y., Yu Q., Hang W. and Huang B. (2010)
Progress of laser ionization mass spectrometry for elemental analysis – A review of the past decade. Spectrochimica Acta Part B, 65, 871–883.

Luque F.J., Rodas M. and Galán E. (1992)
Graphite vein mineralization in the ultramafic rocks of southern Spain: Mineralogy and genetic relationships. Mineral Deposita, 27, 226–233.

Lüthi B. (2008)
Remote sensing of the surface of Titan: Photometric properties, comparison with analogues, and future microscopic observations. PhD Thesis. University of Bern (Bern).

Lykke K.R., Parker D.H., Wurz P., Hunt J.E., Pellin M.J., Gruen D.M., Hemminger J.C. and Lattimer R.P. (1992)
Mass spectrometric analysis of rubber vulcanizates by laser desorption/laser ionization. Analytical Chemistry, 64, 2797–2803.

Majer J.R., Alali B.I. and Azzouz A.S.P. (1981)
The mass-spectrum of glycine. Organic Mass Spectrometry, 16, 147–152.

Managadze G.G., Wurz P., Sagdeev R.Z., Chumikov A.E., Tuley M., Yakovleva M., Managadze N.G. and Bondarenko A.L. (2010)
Study of the main geochemical characteristics of Phobos' regolith using laser time-of-flight mass spectrometry. Solar System Research, 44, 376–384.

Maurice S., Wiens R.C., Saccoccio M., Barraclough B., Gasnault O. and sixty-five others. (2012)
The ChemCam instrument suite on the Mars Science Laboratory (MSL) Rover: Science objectives and mast unit description. Space Science Reviews, 170, 95–166.

McSween H.Y., McNutt R.L. and Prettyman T.H. (2011)
Spacecraft instrument technology and cosmochemistry. Proceedings of the National Academy of Sciences of the United States of America, 108, 19177–19182.

Nakazawa M. and Somorjai G.A. (1993)
Adsorption of substituted benzenes on polycrystalline gold and on zinc oxide and iron oxide overlayers. Applied Surface Science, 68, 517–537.

Neuland M.B., Meyer S., Mezger K., Riedo A., Tulej M. and Wurz P. (2014)
Probing the Allende meteorite with a miniature laser-ablation mass analyser for space application. Planetary and Space Science, 101, 196–209.

Pavlov S.G., Schroder S., Rauschenbach I., Jessberger E.K. and Hubers H.W. (2012)
Low-energy laser induced breakdown spectroscopy for *in-situ* space missions to solar system bodies without atmospheres. Planetary and Space Science, 71, 57–63.

Prettyman T.H. (2006)
Remote chemical sensing using nuclear spectroscopy. In: McFadden L.-A., Weissman P.R. and Johnson T.V. (eds), Encyclopedia of the Solar System. Academic Press (San Diego), 765–786.

Pullan D. (2008)
Analogue studies for *in situ* surface planetary exploration. PhD Thesis. University of Leicester (Leicester).

Pullan D., Westall F., Hofmann B.A., Parnell J., Cockell C.S., Edwards H.G.M., Villar S.E.J., Schroder C., Cressey G., Marinangeli L., Richter L. and Klingelhofer G. (2008)
Identification of morphological biosignatures in martian analogue field specimens using *in situ* planetary instrumentation. Astrobiology, 8, 119–156.

Rauscher H., Jakob P. and Menzel D. (1991)
The adsorption and reaction of toluene on Ru(001), and coadsorption with CO. Surface Science, 256, 27–41.

Riedo A. (2014)
Development and performance analysis of laser ablation mass spectrometer design for space research. PhD Thesis. University of Bern (Bern).

Riedo A., Wahlstrom P., Scheer J.A., Wurz P. and Tulej M. (2010)
Effect of long duration UV irradiation on diamondlike carbon surfaces in the presence of a hydrocarbon gaseous atmosphere. Journal of Applied Physics, 108, 114915, 1–8.

Riedo A., Bieler A., Neuland M., Tulej M. and Wurz P. (2013a)
Performance evaluation of a miniature laser ablation time-of-flight mass spectrometer designed for *in situ* investigations in planetary space research. Journal of Mass Spectrometry, 48, 1–15.

Riedo A., Neuland M., Meyer S., Tulej M. and Wurz P. (2013b)
Coupling of LMS with fs-laser ablation ion source: Elemental and isotope composition measurements. Journal of Analytical Atomic Spectrometry, 28, 1256–1269.

references

Riedo A., Meyer S., Heredia B., Neuland M.B., Bieler A., Tulej M., Leya I., Iakovleva M., Mezger K. and Wurz P. (2013c)
Highly accurate isotope composition measurements by a miniature laser ablation mass spectrometer designed for *in situ* investigations on planetary surfaces. Planetary and Space Science, 87, 1–13.

Rigas P.G. (2012)
Liquid chromatography-post-column derivatization for amino acid analysis: Strategies, instrumentation and applications. Instrumentation Science and Technology, 40, 161–193.

Rohner U., Whitby J.A. and Wurz P. (2003)
A miniature laser ablation time-of-flight mass spectrometer for *in situ* planetary exploration. Measurement Science and Technology, 14, 2159–2164.

Rohner U., Whitby J.A., Wurz P. and Barabash S. (2004)
Highly miniaturized laser ablation time-of-flight mass spectrometer for a planetary rover. Review of Scientific Instruments, 75, 1314–1322.

Russo R.E., Mao X., Gonzalez J.J. and Yoo J. (2013)
Lasers and optics interface – Femtosecond versus nanosecond laser pulse duration for laser ablation chemical analysis. Spectroscopy, 28, 24–39.

Sakairi M. and Yergey A.L. (1991)
Atmospheric-pressure spray and electrospray mass-spectra of glycine and its oligopeptides. Analytical Sciences, 7, 589–592.

Salle B., Lacour J.L., Vors E., Fichet P., Maurice S., Cremers D.A. and Wiens R.C. (2004)
Laser-induced breakdown spectroscopy for Mars surface analysis: Capabilities at stand-off distances and detection of chlorine and sulfur elements. Spectrochimica Acta Part B, 59, 1413–1422.

Salle B., Cremers D.A., Maurice S., Wiens R.C. and Fichet P. (2005)
Evaluation of a compact spectrograph for in-situ and stand-off laser-induced breakdown spectroscopy analyses of geological samples on Mars missions. Spectrochimica Acta Part B, 60, 805–815.

Salle B., Mauchien P. and Maurice S. (2007)
Laser-induced breakdown spectroscopy in open-path configuration for the analysis of distant objects. Spectrochimica Acta Part B, 62, 739–768.

Thomas N., Keller H.U., Arijs E., Barbieri C., Grande M. and thirty-seven others. (1998)
OSIRIS – The optical, spectroscopic and infrared remote imaging system for the Rosetta orbiter. Space Exploration of the Outer Space Solar System and Cometary Nuclei, 21, 1505–1515.

Thomas N., Luthi B.S., Hviid S.F., Keller H.U., Markiewcz W.J., Blumchen T., Basilevsky A.T., Smith P.H., Tanner R., Oquest C., Reynolds R., Josset J.L., Beauvivre S., Hofmann B., Ruffer P. and Pillinger C.T. (2004)
The microscope for Beagle 2. Planetary and Space Science, 52, 853–866.

Tsai M.C. and Muetterties E.L. (1982)
Coordination chemistry of benzene, toluene, cyclohexadienes, cyclohexene, and cyclohexane on platinum (100). The Journal of Physical Chemistry, 86, 5067–5071.

Tulej M., Iakovleva M., Leya I. and Wurz P. (2011)
A miniature mass analyser for *in-situ* elemental analysis of planetary material – Performance studies. Analytical and Bioanalytical Chemistry, 399, 2185–2200.

Tulej M., Riedo A., Iakovleva M. and Wurz P. (2012)
On applicability of a miniaturized laser ablation time of flight mass spectrometer for measurements of trace elements. International Journal of Spectroscopy, 2012, 1–14.

Vertes A., Gijebels R. and Adams F. (1993)
Laser ionisation mass analysis. Wiley (New York, USA), 560pp.

Vilas F., Jarvis K.S. and Gaffey M.J. (1994)
Iron alteration minerals in the visible and near-infrared spectra of low-albedo asteroids. Icarus, 109, 274–283.

Wetterer S.M., Lavrich D.J., Cummings T., Bernasek S.L. and Scoles G. (1998)
Energetics and kinetics of the physisorption of hydrocarbons on Au(111). Journal of Physical Chemistry B, 102, 9266–9275.

Wiens R.C., Maurice S., Barraclough B., Saccoccio M., Barkley W.C. and seventy-five others. (2012)
The ChemCam instrument suite on the Mars science laboratory (MSL) rover: Body unit and combined system tests. Space Science Reviews, 170, 167–227.

Wurz P., Lykke K.R., Pellin M.J., Gruen D.M. and Parker D.H. (1992)
Characterization of fullerenes by laser-based mass spectrometry. Vacuum, 43, 381–385.

Wurz P., Abplanalp D., Tulej M., Iakovleva M., Fernandes V.A., Chumikov A. and Managadze G.G. (2012a)
Mass spectrometric analysis in planetary science: Investigation of the surface and the atmosphere. Solar System Research, 46, 408–422.

Wurz P., Abplanalp D., Tulej M. and Lammer H. (2012b)
A neutral gas mass spectrometer for the investigation of lunar volatiles. Planetary and Space Science, 74, 264–269.

Zelenyi L.M. and Zakharov A.V. (2010)
Phobos-Grunt project: Devices for scientific studies. Solar System Research, 44, 359–361.

Zhang B.C., He M.H., Hang W. and Huang B.L. (2013)
Minimizing matrix effect by femtosecond laser ablation and ionization in elemental determination. Analytical Chemistry, 85, 4507–4511.